Reaction centers of the thermophilic microaerophile, Chloracidobacterium thermophilum (Acidobacteria) I. Biochemical and biophysical characterization

Zhihui He, Bryan Ferlez, Vasily Kurashov, Marcus Tank, John H. Golbeck, and Donald A. Bryant

He, Z., Ferlez, B., Kurashov, V., Tank, M., Golbeck, J. H., & Bryant, D. A. (2019). Reaction centers of the thermophilic microaerophile, Chloracidobacterium thermophilum (Acidobacteria) I: biochemical and biophysical characterization. *Photosynthesis research*, *142*(1), 87-103.

Reaction centers of the thermophilic microaerophile, *Chloracidobacterium thermophilum* (*Acidobacteria*)

I. Biochemical and biophysical characterization

*Zhihui He[1], Bryan Ferlez[1,†], Vasily Kurashov[1], Marcus Tank[1,‡], John H. Golbeck[1,2], and Donald A. Bryant[1,3,]**

[1]Department of Biochemistry and Molecular Biology and [2]Department of Chemistry, The Pennsylvania State University, University Park, PA 16802 USA; [3]Department of Chemistry and Biochemistry, Montana State University, Bozeman, MT 59717 USA

To whom correspondence should be addressed: Dr. Donald A. Bryant, S-002 Frear Building, Department of Biochemistry and Molecular Biology, The Pennsylvania State University, University Park, PA 16802 USA. e-mail: dab14@psu.edu; phone (+1)-814-865-1992; fax: (+1) 814-863-7024

[†]**Present Address:** MSU-DOE Plant Research Laboratory, Michigan State University, 612 Wilson Road, East Lansing, MI 48824 USA

[‡]**Present Address:** Department of Biological Sciences, Tokyo Metropolitan University, 1-1 Minami-Osawa, 192-0397, Hachioji, Tokyo, Japan

Keywords: Photosynthesis, chlorophototrophy; Zn-bacteriochlorophyll; type-1 reaction center; anoxygenic photosynthesis; transient electron paramagnetic resonance

Abstract

Chloracidobacterium thermophilum is a microaerophilic, anoxygenic member of the green chlorophototrophic bacteria. This bacterium is the first characterized oxygen-requiring chlorophototroph with chlorosomes, the FMO protein, and homodimeric type-1 reaction centers (RCs). The RCs of *C. thermophilum* are also unique because they contain three types of chlorophylls, bacteriochlorophyll a_P esterified with phytol, Chl a_{PD} esterified with Δ2,6-phytadienol, and Zn-BChl a_P' esterified with phytol, in the approximate molar ratio 32:24:4. The light-induced difference spectrum of these RCs had a bleaching maximum at 839 nm and also revealed an electrochromic bandshift that is probably derived from a BChl *a* molecule near $P840^+$. The F_X [4Fe-4S] cluster had a midpoint potential of *ca.* –581 mV, and the spectroscopic properties of the P^+ F_X^- spin-polarized radical-pair were very similar to those of reaction centers of heliobacteria and green sulfur bacteria. The data further indicate that electron transfer occurs directly from A_0^- to F_X, as occurs in other homodimeric Type-1 RCs. Washing experiments with isolated membranes suggested that the PscB subunit of these reaction centers is more tightly bound than PshB in heliobacteria. Thus, the reaction centers of *C. thermophilum* have some properties that resemble other homodimeric reaction centers but also have specific properties that are more similar to those of Photosystem I. These differences probably contribute to protection of the electron transfer chain from oxygen, contributing to the oxygen tolerance of this microaerophile.

Abbreviations: BChl, bacteriochlorophyll; BPheo, bacteriopheophytin; *C.*, *Chloracidobacterium*; *Cba.*, *Chlorobaculum*; Chl, Chlorophyll; CW-EPR, continuous wave, field-modulated, time-resolved continuous-wave electron paramagnetic resonance; β-DDM, *n*-dodecyl-β-maltoside; EPR, electron paramagnetic resonance; FMO, Fenna-Matthews-Olson bacteriochlorophyll *a*-binding protein; HEPES, 4-(2-hydroxyethyl)piperazine-1-ethanesulfonic acid; HPLC, high performance liquid chromatography; 2D-HYSCORE, two-dimensional hyperfine sublevel correlation spectroscopy; LC-MS-MS, liquid chromatography-tandem mass spectrometry; LED, light-emitting diode; OD, optical density; P, phyol; PAGE, polyacrylamide gel electrophoresis; PBS, phosphate-buffered saline; PD, 2,6-phytadienol; Pheo, pheophytin; photo-CIDNP, photochemically induced dynamic nuclear polarization; PSI, photosystem I; PSII, photosystem II; RC(s), reaction center(s); RP, reversed phase; SDS, sodium dodecyl sulfate; SHE, standard hydrogen electrode; trEPR, transient electron paramagnetic resonance; ZFS, zero field splitting

INTRODUCTION

Chloracidobacterium (*C.*) *thermophilum* is the first, and to date the only, chlorophototrophic member of the phylum *Acidobacteria* (Bryant et al., 2007; Tank and Bryant, 2015a, b; Tank et al., 2018; Thiel et al., 2018). Physiologically, *C. thermophilum* is a microaerophilic, anoxygenic member of the green bacteria, and like other green bacteria, it employs chlorosomes, in this case containing bacteriochlorophyll (BChl) *c,* as the major light-harvesting antenna (Garcia Costas et al., 2011, 2012b; Thweatt et al., 2019). The remaining photosynthetic apparatus of *C. thermophilum* most closely resembles that of green sulfur bacteria. The BChl *a*-binding Fenna-Matthews-Olson protein serves as an intermediate in energy transfer from chlorosomes to its type-1 homodimeric reaction centers (RCs) in the cytoplasmic membrane (Tsukatani et al., 2010; Wen et al., 2011).

C. thermophilum is incapable of photoautotrophic growth and cannot synthesize vitamin B_{12}, lysine or branched-chain amino acids, although it can degrade the latter (Garcia Costas et al., 2012; Tank and Bryant, 2015a, b; Tank et al., 2018). *C. thermophilum* requires oxygen for growth, but it is a microaerophile and is unable to grow at atmospheric levels of oxygen (Tank and Bryant, 2015a, b). Although *C. thermophilum* is unable to grow autotrophically, it nevertheless obligately requires bicarbonate for growth, possibly because cells may carboxylate succinyl-CoA produced by degradation of amino acids to synthesize 2-oxoglutarate, the precursor metabolite for BChl biosynthesis. *C. thermophilum* additionally is unable to fix dinitrogen or reduce nitrate, and it requires reduced sulfur compounds as sulfur source (e.g., cysteine, methionine or thioglycolate). *C. thermophilum* can assimilate all of the twenty common amino acids except L-aspartate and L-glutamate (Tank and Bryant, 2015a, b). This unusual combination of physiological and metabolic traits is unique among chlorophototrophic bacteria (Thiel et al., 2018).

RCs are the essential components of (bacterio)-chlorophyll- [(B)Chl]-based chlorophototrophy because they are responsible for converting light energy into stored chemical potential energy. RC complexes are classified into two types on the basis of their terminal electron acceptors (Golbeck, 1993; Sadekar et al., 2006; Cardona et al., 2015). Type-1 RCs produce weak oxidants and strong reductants, and they utilize Fe/S clusters as terminal electron acceptors. Photosystem I (PSI) of cyanobacteria and higher

plants is an example of a heterodimeric, type-1 RC (Nitschke and Rutherford, 1991; Golbeck and Bryant, 1991; Jordan et al., 2001; Golbeck, 1993; Grotjohann and Fromme, 2005). Homodimeric type-1 RCs occur in chlorophototrophs belonging to three bacterial phyla: the strictly anaerobic, photoheterotrophic heliobacteria (*Firmicutes*); chlorophototrophic members of the phylum *Chlorobi*; and *C. thermophilum* (*Acidobacteria*) (Bryant et al., 2007; Thiel et al., 2018; Thweatt et al., 2019). The first X-ray structure of a homodimeric RC was very recently described for a heliobacterium, *Heliobacterium* (*H.*) *modesticaldum* (Gisriel et al., 2017).

Type-2 RCs produce strong oxidants and weak reductants, and they use quinones as terminal electron acceptors. Purple bacteria (*Proteobacteria*), filamentous anoxygenic phototrophs (*Chloroflexi*), and *Gemmatimonas phototrophica* (*Gemmatimonadetes*) contain heterodimeric type-2 RCs (Bryant and Frigaard, 2006; Sadekar et al., 2006; Zeng et al., 2014; Thiel et al., 2018; Thweatt et al., 2019). *Hymenobacter* sp. isolate R-68361 may be the first member of the phylum *Bacteroidetes* that can produce type-2 RCs (Tahon and Willems, 2017; Thiel et al., 2018). Plants and cyanobacteria employ Photosystem II (PSII), also a type-2 RC, in series with PSI to oxidize water, evolve oxygen, and produce NADPH and protonmotive force for ATP synthesis (Golbeck 1993; Bryant, 1994; Shen, 2016). The primary electron acceptor for all type-2 RCs is either a bacteriopheophytin (BPheo) in the RCs of anoxygenic bacteria or pheophytin (Pheo) *a* in the case of PSII (Sadekar et al., 2006; Cardona et al., 2015).

Currently, *C. thermophilum* and "*Candidatus* Thermochlorobacter aerophilum" are the only described microaerophilic or aerobic chlorophototrophs, respectively, that have type-1 RCs (Liu et al. 2012; Tsukatani et al. 2012; Tank et al., 2017; Thiel et al., 2018). "*Ca*. T. aerophilum" can only be grown in enrichment cultures with other phototrophs (Tank et al., 2017), making a determination of its RC properties challenging. Metagenomic sequence data, generated from the hot spring microbial mats in which *C. thermophilum* occurs (Bryant et al., 2007; Ward et al., 2017), as well as the complete genome sequence of this organism (Garcia Costas et al., 2012a) revealed the presence of an operon containing the *pscA, pscB,* and *fmoA* genes, which respectively encode the homodimeric RC core subunit (PscA); the PscB subunit that is predicted to harbor two [4Fe-4S] (F_A/F_B-like) clusters of a type-1 RC; and the FMO apoprotein

(FmoA), respectively (Bryant et al. 2007). Because *C. thermophilum* is an obligate chlorophototroph and must be cultivated under microoxic conditions, it follows that its RCs are assembled and must be stable under microoxic conditions. These and other properties make these RCs a unique system for investigating electron transport in homodimeric type-1 RCs. Information gained from such studies may contribute new insights into the evolutionary events that led from anoxygenic to oxygenic photosynthesis.

(B)Chls perform multiple functions in the RCs of chlorophototrophs: they act as light-harvesting antenna molecules and transfer excitation energy to other (B)Chls that participate in electron transfer as electron donors and acceptors. Previous studies of the RCs of *C. thermophilum* by reversed-phase high-performance liquid chromatography (RP-HPLC) revealed the presence of three types of (B)Chls: BChl a_P, Chl a_{PD}, and Zn-BChl a_P' in an approximate ratio 12.8:8.0:2.0 (Tsukatani et al. 2012). These findings were surprising for two reasons: (1) no other type-1 RCs contain more than two types of (B)Chls; and (2) very few organisms have been described that naturally produce Zn-BChl *a* (Wakao et al., 1996; Tomi et al., 2007). Chl a_{PD} was identified as the primary electron acceptor in a recent study of ^{15}N-labeled RCs of *C. thermophilum* by photochemically induced dynamic nuclear polarization (photo-CIDNP; Zill et al. 2018). Zn-BChl a_P' was only found in the RCs (Tsukatani et al., 2012) and was not present in chlorosomes (Garcia Costas et al., 2011, 2012b) nor in the FMO antenna protein that only contained Mg-BChl a_P (Tsukatani et al. 2010; Wen et al. 2011). This led to the hypothesis that Zn-BChl a_P' was the primary electron donor in the RCs of *C. thermophilum*. In this study we describe additional biochemical and biophysical properties of the RCs of *C. thermophilum*, which establish key similarities and differences compared to other type-1 RCs. In a companion study that will be published in detail elsewhere, ^{67}Zn-hyperfine sublevel correlation (^{67}Zn-HYSCORE) spectroscopy was performed, and those studies establish clearly that the primary electron donor, P_{840}, of the *C. thermophilum* RC is a dimer of Zn-BChl a_P' (for a preliminary report, see Charles et al., 2019).

MATERIALS AND METHODS

Medium preparation and growth of *C. thermophilum* cells

C. thermophilum strain B^T was grown in CTM medium according to the procedures described in Tank and Bryant (2015a, b). Slight changes in the medium were made to achieve growth of *C. thermophilum* on a medium containing ^{67}Zn. The $ZnSO_4$ in the CTM medium was replaced by 7 μM $^{67}ZnCl_2$, which was produced by dissolution of ^{67}Zn metal in 12 N HCl (Trace Sciences International Corp, Pilot Point, TX). Cells were incubated at 53 °C in sealed bottles under microoxic conditions in an orbital shaking incubator (75 rpm) and were illuminated with a tungsten lamp at 50 μmol photons m^{-2} s^{-1} for 7 to 10 days prior to cell harvesting by centrifugation. Cells were stored at –80 °C until required.

Absorbance spectra and polyacrylamide gel electrophoresis

Absorbance spectra were recorded with a Genesys 10 spectrophotometer (ThermoFisher Scientific, Waltham, MA). Polyacrylamide gel electrophoresis in the presence of sodium dodecyl sulfate (SDS-PAGE) was performed as previously described (Shen and Bryant 1995). The stacking gel contained 4% (w/v) acrylamide, and the resolving gel contained 15% (w/v) acrylamide (30.0:0.8 w/w, acrylamide: *N, N′*-methylenebisacrylamide). Gels were stained with Coomassie Brilliant Blue R-250 or silver as described (Blum et al., 1987).

Preparation of washed membranes from *C. thermophilum*

Washed membranes from *C. thermophilum* were purified by a method reported previously with some modifications (Zill et al. 2018). *C. thermophilum* cells (from 5 L of culture; ~30 g wet weight) were harvested by centrifugation at 7,500 × *g* for 60 min. Cell pellets were resuspended in 60 ml of 50 mM 4-(2-hydroxyethyl)piperazine-1-ethanesulfonic acid (HEPES) buffer (pH 7.0) containing 1 mM phenylmethylsulfonyl fluoride, 2 mM dithiothreitol, and 3 mg of lysozyme ml^{-1}. The suspensions were incubated at room temperature in the dark for 30 min. The cell suspensions were kept on ice while the treated cells were disrupted by four passages through a chilled French pressure cell at 138 MPa. Unbroken cells and large cell debris were removed by centrifugation at 8,000 × *g* for 10 min, and the resulting supernatant was subjected to centrifugation at 220,000 × *g* for 1.5 h. The resulting pellet was resuspended in phosphate-buffered saline (PBS = 10 mM potassium phosphate pH 7.2, 150 mM NaCl) to an OD_{810} of 8

cm^{-1}. In some cases as specified, the pellet was resuspended in PBS containing 0.6 M Na-carbonate, and the membrane suspension was incubated overnight at 4 °C. This treatment released FMO and PscB from the membranes (see Results). Chlorosome-depleted membranes were isolated on 10 to 50% (w/v) sucrose density gradients, which separated the greenish-brown, chlorosome-containing fraction from the orange-colored membranes that contained FMO and RCs (Fig. S1).

For electron paramagnetic resonance (EPR) measurements, chlorosome-depleted membranes ($OD_{810\,nm}$ = 2.0) that had been washed with phosphate-buffer saline (PBS, 10 mM potassium phosphate pH 7.2, 150 mM NaCl) were incubated with 30 mM sodium ascorbate (for as-isolated samples) or 50 mM dithionite (final concentration) from a concentrated stock solution prepared in 1.0 M glycine buffer, pH 10.0 (for reduced samples) for 10 min in the dark prior to freezing. Membranes from *C. thermophilum* cells that had been treated with 2.0 M sodium thiocyanate were prepared as described by Tsukatani et al. (2012) and incubated with 30 mM sodium ascorbate as described above.

Purification of RC complex from *C. thermophilum*

Concentrated membranes (12 ml, OD_{810} = 8) were solubilized by adding *n*-dodecyl-β-maltoside (β-DDM; 10% w/v stock solution) to the suspension to a final β-DDM concentration of 1% (w/v). The mixture was incubated at 4 °C for 1 h, and insoluble material was removed by centrifugation at 200,000 × *g* for 1 h. Solubilized membranes were loaded onto 5 to 25% (w/v) linear sucrose density gradients from prepared in 50 mM HEPES buffer (pH 7.0) containing 0.03% (w/v) β-DDM. After centrifugation at 220,000 × *g* for 18 h at 4 °C, the intensely orange carotenoid binding protein fraction was separated from a grayish-brown-colored RC-FMO fraction (see Fig. 1a); this fraction was collected, diluted with the same buffer, and concentrated by ultrafiltration (50-kDa molecular mass cutoff; Millipore, Billerica, MA). In some cases, a second sucrose density gradient was used to further reduce contamination from the carotenoid binding protein (see Fig. 2a, b).

The grayish-brown-colored RC-FMO fraction was collected and subjected to anion-exchange chromatography on a DEAE-Sepharose column (2.5 × 4 cm) equilibrated with 50 mM HEPES buffer, pH

7.0, containing 0.03% (w/v) β-DDM. The grayish-brown-colored RC fraction was eluted with 50-100 mM NaCl. Fractions enriched in RC were pooled and concentrated by ultrafiltration (50-kDa molecular mass cutoff; Millipore, Billerica, MA). This method could remove most of the FMO protein and most other contaminating proteins from the RC fraction.

Trypsin digestion and protein identification

Tryptic peptide mass fingerprinting analyses were performed by digesting protein solutions directly or by digesting polypeptides in slices excised from polyacrylamide gels. For in-solution digestion, digestion buffer (25 mM ammonium bicarbonate, 15 μl) was mixed with reducing reagent (3 μl, 5 mM *tris*-(2-carboxyethyl) phosphine hydrochloride solution in 25 mM ammonium bicarbonate) and protein solution (12 μl). The mixture was incubated at 60 °C for 5-10 min to reduce the proteins, and alkylation was performed by adding the alkylating reagent (3 μl, 100 mM iodoacetamide solution in 25 mM ammonium bicarbonate) to the solution, which was then incubated at room temperature for 20 min. The detergent was removed by washing the proteins five times using centrifugal ultrafiltration devices (EMD Millipore, Darmstadt, Germany). The resulting solution was treated overnight with activated trypsin (5 μl, 0.1 μg μl^{-1} in 25 mM ammonium bicarbonate) at 37 °C, stored at –20 °C until required for LC-MS-MS analysis.

Polypeptides in gel slices were digested with trypsin as follows. Gel slices that had been stained with Coomassie Brilliant Blue were dices into small cubes. The gel cubes were washed three times with 25 mM ammonium bicarbonate in 50% (v/v) acetonitrile by incubation at 37 °C for 15-20 min. The supernatant for each sample was discarded, and the gel slices were covered with 5 mM *tris*-(2-carboxyethyl)phosphine hydrochloride solution in 25 mM ammonium bicarbonate at 60 °C for 10 min. The supernatants were discarded, and the gel slices were treated with 100 mM iodoacetamide solution in 25 mM ammonium bicarbonate in the dark at 37 °C for 15 min. The supernatant solutions were discarded, and the gel slices were washed three times with 25 mM ammonium bicarbonate, dehydrated with 25 mM ammonium bicarbonate in 50% (v/v) acetonitrile, and were air-dried at room temperature. The gel samples were incubated with trypsin solution (10 ng of trypsin μl^{-1} in 25 mM ammonium bicarbonate; Promega) at 37 °C

for 16 h. The digested peptides were extracted with acetonitrile containing 0.1 % (v/v) formic acid by incubation at 37 °C for 15 min. This step was repeated twice, and a final extraction was performed with 100% acetonitrile. The pooled extracts were evaporated under vacuum and analyzed by LC-MS-MS, which was performed in the Proteomics and Mass Spectrometry Facility at the Huck Institutes for the Life Sciences at The Pennsylvania State University.

Measurement of light-induced difference spectra

A laboratory build setup was used to measure the light-induced difference spectra. Varian Cary 50 UV-Vis spectrophotometer was used to measure the absorbance of the sample while a Newport 66902 arc lamp housing outfitted with a 400 W xenon lamp acted as the actinic light source. The actinic light was first passed through a circulating water filter to reduce sample heating. An optical fiber with an outboard shutter directed the light to the cuvette holder at a 90° angle to the probe beam. The absorbance of the sample was measured at a given wavelength with the shutter closed for 2 min (the dark signal) and with the shutter open (the light signal); the difference between the light and dark signals was plotted against the corresponding wavelength. A recovery period necessary for the system to return to the ground state followed each measurement. The sample was placed in a 0.4 cm × 1.0 cm cuvette that was oriented so that the measuring beam passed through the 1 cm optical path and the actinic beam passed through the 0.4 cm path. The light intensity was adjusted by altering the voltage to the lamp to achieve the minimum saturating power, *i.e.* the power at which any further increase in the light intensity showed no increase in the absorbance change. The measurements were performed in presence of 10 mM sodium ascorbate. The sample was made anaerobic immediately before the measurement by purging the overhead space with argon for 1 hour.

High performance liquid chromatography

The pigment composition of RC preparations was determined by RP-HPLC on an Agilent 1100 HPLC system (Agilent Technologies) equipped with an analytical Discovery C18 column (4.6 mm × 25 cm) (Supelco, Sigma-Aldrich) as described (Frigaard et al., 1997). The gradient was composed of Solvent A (42% methanol, 33% acetonitrile, 25% water (v/v/v)) and Solvent B (50% methanol, 20% acetonitrile, 30%

ethyl acetate (v/v/v)). At the time of injection, the mobile phase was 30% Solvent B at a flow rate of 1 ml min^{-1}. Solvent B was linearly increased to 100% over 50 min; this was followed by a constant flow of 100% Solvent B for 8 min after which Solvent B was returned to 30% in 2 min.

Low-temperature CW X-band EPR spectroscopy

Low-temperature, continuous-wave (CW)-EPR spectroscopy was performed at X-band using an E-500 ELEXSYS EPR spectrometer (Bruker BioSpin Corp., Billerica, MA). The sample was dark adapted with 1 mM ascorbate for 1 hour and then frozen in the dark in liquid nitrogen. The measurements were conducted in the Super-hi-Q cavity (Bruker BioSpin Corp., Billerica, MA) with an ESR 900 cryostat (Oxford Instruments, Concord, MA). A Verdi V5 532 nm CW laser (Coherent, Inc., Santa Clara, CA) equipped with a 3-fold beam expander (Oriel Instruments, Irvine, CA) was used to illuminate the sample inside the cavity.

Low-temperature transient X-band EPR spectroscopy

Transient electron paramagnetic resonance (trEPR) measurements were made using a modified Bruker E300 EPR spectrometer at X-band in direct detection mode. A Flexline dielectric resonator (ER 4118 X-MD-5W1, Bruker BioSpin Corp., Billerica, MA) was used, and the temperature was maintained at 90 K with an ER 4118CF liquid helium cryostat (Bruker BioSpin Corp., Billerica, MA) and an ITC-4 controller. The trEPR signal was collected with a home-built broadband amplifier (bandwidth >500 MHz) and digitized using a 500 MHz bandwidth, 8-bit, 2GS/s, Model CS85G PCI card (DynamicSignals LLC, Lockport, IL). The software for controlling the spectrometer and for data acquisition was written in-house in LabView. Three-dimensional time/field/amplitude data sets were collected following single-turnover flashes at 20 mJ per pulse from a Vibrant 355II laser (Opotek, Inc., Carlsbad, CA) running at 10 Hz and a wavelength of 532 nm with a pulse width of 7 ns. Each time/field data set consists of 128 to 512 trEPR signals collected and averaged at each fixed magnetic field at a resolution of 0.5 mT for triplet spectra and 25 μT for RP spectra. Boxcar spectra were extracted from the field/time data sets by integrating the EPR signal between 1 and 2 μsec following the laser flash.

Optical sample preparation, data collection, and analysis

Time-resolved absorbance changes at 840 nm were measured at room temperature using a commercial JTS-10 pump-probe spectrometer with a path length of 1 cm (Biologic LLC). A pulsed Nd:YAG laser with a pulse width of ~ 400 ns and a single-pulse energy of ~3.0 mJ/pulse at 532 nm (Clark MXR ORC-1000) provided the actinic flashes. Detection light was provided by the built-in, pulsed 810-nm light-emitting diode (LED) filtered at 840 nm using an interference filter (FWHM = 10 nm) (Edmund Optics, Barrington, NJ). Data represent the average of either 16 (oxic conditions) or 1 (anoxic conditions) light-minus-dark, single-turnover events; the dark data set was collected following each actinic collection by physically blocking the actinic light from reaching the sample while still firing the laser. This was done to subtract an electrical artifact generated by the Q-switch operation of the laser. Data collection began 300 μsec after the actinic flash due to prevent interference from stray actinic laser light reaching the detector. The decay kinetics at 840 nm were fit using a non-linear, least-squares multi-exponential fitting algorithm in Igor Pro (Wavemetrics, Lake Oswego, OR).

Sodium chloride, sodium carbonate and sodium thiocyanate washes of membranes

The following optical experiments were carried out at room temperature using chlorosome-depleted membranes ($OD_{810\ nm}$ = ~0.6) and in the presence of 30 mM sodium ascorbate. Oxic membranes of *C. thermophilum* that had been washed with PBS were degassed with argon at 6 psi for 15 min to remove oxygen. Anoxic time-resolved, charge-recombination kinetics at 840 nm were then measured using the same instrumentation described above (see Results). An aliqot (3.0-ml) of these anoxic, PBS-washed membranes was diluted 22-fold in PBS, and the membranes were pelleted by ultracentrifugation at 207,000 × *g* for 30 minutes at 4 °C. The supernatant was discarded, and the resulting pellet was resuspended in 3 ml of 100 mM sodium carbonate buffer at pH 11.5 containing 500 mM NaCl in attempt to remove PscB from the RC. After a 30-min incubation in the sodium carbonate/NaCl buffer at 4°C, the membranes were again diluted 22-fold in PBS buffer and pelleted by ultracentrifugation as described above. The supernatant was again discarded and the resulting membrane fraction was resuspended in 3.0 ml of PBS buffer and degassed

with argon at 6 psi for 15 min prior to measuring the time-resolved, charge-recombination kinetics at 840 nm (see Results). Finally, the membranes were again pelleted by ultracentrifugation and resuspended in PBS buffer (3.0 ml) containing 1 M sodium thiocyanate. The sample was degassed to remove oxygen, and the time-resolved, charge-recombination kinetics at 840 nm were measured after incubation of the membranes for 30-min or 1.0 h in the PBS-thiocyanate buffer (see Results).

Redox titration of *C. thermophilum* membranes

Redox titration of chlorosome-depleted membranes of *C. thermophilum* at room-temperature was carried out as described by Ferlez et al. (2016). Briefly, an anoxic master mix of PBS-washed, chlorosome-depleted membranes and electron mediators (methyl viologen, benzyl viologen, dimethyl triquat, and triquat) in 100 mM glycine buffer at pH 10.0 was poised at solution potentials ranging from –283 mV to – 592 mV versus the standard hydrogen electrode (SHE) by adding small aliquots of concentrated sodium dithionite (~500 mM) in 1.0 M glycine buffer pH 10.0 or 100 mM potassium ferricyanide in PBS buffer. The solution potential was measured using a high-impedance digital voltage meter that connected to a gold working electrode and an Ag/AgCl reference electrode (Microelectrodes Inc., Bedford, NH), which was calibrated using a saturated solution of quinhydrone. After addition of dithionite or ferricyanide, the solution potential was allowed to stabilize until the potential no longer changed, typically 5-10 min. At this time, an aliquot (120 µl) of membranes of the master mix was removed, rapidly transferred rapidly to an EPR tube and flash-frozen in liquid nitrogen. This procedure was repeated until samples spanning the potential range from about –300 to –600 mV (*vs.* SHE) were prepared. Samples were stored in liquid nitrogen until analysis. The trEPR spectra were subjected to a linear baseline correction and the amplitudes of the absorptive features fit using the Nernst equation and a non-linear, least-squares fitting algorithm in Igor Pro (Wavemetrics, Lake Oswego, OR).

RESULTS

Membrane and RC preparations

Depending upon the experiments to be performed, different types of membranes and RC complexes derived from detergent-solubilized membranes of *C. thermophilum* were prepared for analysis. Crude membranes are generally not suitable for most experiments described here because of the strong absorption of light by chlorosomes at ~743 nm (see Fig. S1a). Chlorosomes contain very large amounts of BChl *c* (Bryant and Canniffe, 2018), and they interfere with light-activated or optically detected processes. To circumvent this problem, membranes were washed with PBS buffer to remove most of the chlorosomes (see Materials and Methods; Fig. S1a, S1b). This washing step releases >90% of the chlorosomes, which could be separated from the RC-containing membrane fraction on sucrose density gradients (see Fig. S1), but this washing step did not remove the BChl *a*-binding FMO protein, which can still be detected in these washed membranes by its absorbance maximum at 798 nm (Figs. S1b**)** (Tsukatani et al., 2010; Wen et al., 2011).

Detergent solubilization of PBS-washed membranes followed by one or occasionally two rounds of sucrose gradient centrifugation (Fig. 1) led to fractions from which the carotenoid binding protein had been removed (Fig. 1a, 1b). These RC preparations still contained the FMO protein and retained the PscB protein (Fig. 1b). However, the PscB protein appeared to be sensitive to proteolysis and was usually detected as several polypeptide bands by tryptic peptide mass fingerprinting analysis (data not shown). Ion-exchange chromatography on diethylaminoethyl (DEAE)-cellulose was effective in removing a number of contaminating proteins, including the FMO protein, but this procedure removed all of the PscB subunit (data not shown).

A different procedure was used to wash the membranes and remove FMO completely. Prior to solubilization, the membranes were washed with 0.6 M Na-carbonate buffer at pH 7.2. This wash step efficiently removes the FMO protein, but it also completely removes the PscB subunit from the RCs (Figs. 2a-d). After detergent solubilization of these membranes, the carotenoid binding protein (CbpA; see Tsukatani et al., 2012) could be removed by two rounds of sucrose gradient centrifugation (Fig. 2a, 2b). RC preparations of this type were completely devoid of contaminating FMO but contained several minor polypeptides between 10 and 25 kDa in addition to the core homodimer, PscA = Cabther_A2188 (Fig. 2c, 2d). The polypeptide with an apparent mass of about 15 kDa is the product of Cabther_A2183 (Fig. 2d;

Table S1). This ORF is predicted to encode a membrane-anchored, cytochrome *c* lipoprotein with a single heme group, and interestingly, it is encoded in the same operon as *pscA-pscB-fmoA* (Fig. 2e). The protein with an apparent mass of ~16 kDa is the product of Cabther_A2184, also predicted to encode a membrane-anchored, cytochrome *c* lipoprotein with one heme group, and it is also encoded in the same operon as *pscA-pscB-fmoA* (Fig. 2e). The polypeptide with an apparent mass of 25 kDa may represent a residual amount of the carotenoid-binding protein, CbpA, which migrates anomalously during SDS-PAGE (Tsukatani et al, 2012). The identities of the remaining proteins are unknown, but one or more could be derived from residual PscB. Polypeptides with apparent masses of ~10 kDa were also often observed, but tryptic peptide mass fingerprinting of this band from multiple preparations failed to identify a consensus protein. This band appeared to contain polypeptide fragments derived from proteolytic degradation of some of the larger proteins in the sample. Peptides derived from PscA, FmoA, and the two lipoprotein cytochromes mentioned above, as well as other proteins, were sometimes identified when this band was analyzed by mass spectrometry.

The absorbance spectrum of an RC preparation completely devoid of contaminating FMO is shown in Fig. 3. This spectrum clearly lacks the absorbance peak at 798 nm that is characteristic of FMO (Tsukatani et al., 2010; compare Figs. 1c and 3), and instead shows absorbance maxima at 812, 673, and 601 nm as well as a distinctive shoulder at 825 nm. Several additional absorbance maxima are observed in the 350 to 550 nm wavelength range due to the Soret absorbance bands of (B)Chls and the presence of carotenoids in the RC complex. Consistent with previous results (Tsukatani et al., 2012), reversed-phase HPLC and LC-MS analyses of the major fractions revealed the presence of three major Chls, BChl a_P, Chl a_{PD}, and Zn-BChl a_P' (Fig. 4). Chl a_P was usually observed and comprised up to 10% of the total Chl *a* fraction (see Fig. 4). In some preparations, minor species with absorption spectra similar to that of BChl *a* were observed at elution times earlier than that of BChl *a*; we attribute these minor peaks to BChl *a* esterified with alcohols containing more double bonds than phytol (e.g., geranylgeraniol, dihydrogeranylgeraniol, and tetrahydrogeranylgeraniol). The approximate ratio of BChl a_P : Chl a_{PD} + Chl a_P : Zn-BChl a_P' was 7.1 : 5.4 : 1. Assuming that the pigment content is similar to that of the homodimeric

RC of *H. modesticaldum* (Gisriel et al., 2017), the pigment ratios suggest that there might be approximately 4 Zn-BChl a_P' molecules per RC and about 56 remaining (B)Chls per RC monomer. Thus, we estimate that RCs of *C. thermophilum* contain approximately 32 BChl a_P, 24 Chl a_{PD} and 4 Zn-BChl a_P'. This calculation assumes that there are 4 Zn-BChl a_P' molecules, and 56 total Chls with a BChl a_{PD}: Chl a_{PD} + Chl a_P ratio of 1.33.

High-resolution difference spectrum of the primary donor P_{840}

A high-resolution (~1-nm resolution) light-induced difference spectrum of the primary electron donor in *C. thermophilum* RCs is shown in Fig. 5. The measurements were carried out under anoxic conditions, which minimized degradation of the sample from the repeated light-on and light-off cycling. The bleaching around 840 nm is similar to that reported previously by our groups for preparations of *C. thermophilum* RCs, but the features between 750 nm and 825 nm are much better resolved in Fig. 5 than was the case in the initial study (Tsukatani et al., 2012). The point-by-point spectrum was measured at room temperature at wavelengths from 675 nm to 920 nm, with finer resolution from 820 to 850 nm (Fig. 5, inset). The maximal photobleaching occurs near 839 nm (hereafter P_{840}), which is characteristic of a BChl *a*-like molecule and not Chl *a*, in this instance specifically the Zn-BChl a_P' special pair (Charles et al., 2019). Secondary bleaching maxima occur at 795 and 824 nm, similar to those observed earlier in Photosystem I from spinach (Schaffernicht and Junge, 1981, Hiyama and Ke, 1972) and *Anabaena variabilis* (Hiyama and Ke, 1972). These secondary bleachings can be explained by an electrochromic bandshift of a nearby (B)Chl molecule that results from the local electric field created by charge separation on the primary donor. Considering that this bandshift is centered at about 815 nm, it is also likely due to BChl *a* and not Chl *a*.

Charge recombination kinetics between P_{840}^+ and the reduced FeS clusters

The charge recombination kinetics of chlorosome-depleted *C. thermophilum* membranes measured at 840 nm at room temperature under anoxic conditions are depicted in Fig. 6a (see Table S2 for errors associated with the fitted parameters). The slow kinetic phase with a lifetime (relative amplitude) of 156 ms (47%) is

assigned to charge recombination between P_{840}^+ and $[F_A/F_B]^-$, the FeS clusters bound by PscB. The comparable recombination reaction occurs with a lifetime of ~60 ms in PSI (Vassiliev et al., 1997) and ~70 ms in *H. modesticaldum* (Heinnickel and Golbeck, 2007). The fast-kinetic phase with a lifetime (relative amplitude) of 21 ms (53%) is assigned to charge recombination between P_{840}^+ and F_X^-. The comparable recombination reaction occurs with a lifetime of ~1.5 ms in PSI (Vassiliev et al., 1997) and ~15 ms in heliobacterial RCs (Heinnickel and Golbeck, 2007). The biphasic decay may due be to (i) inefficient electron transfer past F_X in fully intact RCs, or (ii) to equilibrium between F_X and F_A/F_B as a result of similar midpoint potentials, or (iii) it may represent subpopulations of RCs with and without PscB. When air was introduced into the sample, the fast (τ =19 ms) and slow (τ =118 ms) kinetic phases were still present, consistent with retention of the F_X^- and $[F_A/F_B]^-$ charge recombination channels, but an additional 3-s kinetic phase appeared at the expense of a fraction of the 118 ms phase (not shown). This component, which had a relative amplitude of 20% of the total absorption change, is assigned to the reduction of P_{840}^+ by sodium ascorbate in those RCs in which the electron has been transferred from $[F_A/F_B]^-$ to O_2.

The charge recombination kinetics of *C. thermophilum* membranes after treatment with 500 mM NaCl and 100 mM sodium carbonate are shown in Fig. 6b. This chemical treatment was intended to remove PscB from the RCs. However, no significant change in the ratio of the fast (τ = 23 ms, 58%) to slow (τ = 342 ms, 42%) kinetic phases were detected, indicating that the treatment was ineffective in removing additional PscB from the RC. This result is in contrast to *H. modesticaldum* and *Chlorobaculum* (*Cba.*) *tepidum,* for which ionic strengths of 0.1 M NaCl and 0.5 M NaCl are sufficient to remove PshB and PscB from the respective RCs (Jagannathan and Golbeck, 2008). The charge recombination kinetics after a 30-minute exposure to 1.0 M NaSCN are shown in Fig. 6c. This treatment was employed in an attempt to remove PscB from the RC. The relative amplitude of the fast (τ = 30 ms) kinetic phase increased to 65% and the relative amplitude of the slow (τ = 242 ms) kinetic phase decreased to 35% without any loss in total signal amplitude. These data suggest that high concentration of chaotropes are partly effective at removing additional PscB, resulting in additional charge recombination from F_X^-. The charge recombination kinetics

after exposure to 1.0 M NaSCN for 1 hour are shown in Fig. 6d. The relative amplitude of the slow (τ = 349 ms) kinetic phase has increased to 41% and the relative amplitude of the fast (τ = 36 ms) kinetic phase has decreased to 59%, but this change was accompanied by a significant reduction in the total signal amplitude. This implies either that charge separation is increasingly inhibited or that charge recombination is occurring from an acceptor prior to F_X. Were the latter to have a lifetime <300 μsec, it would not be resolved by our instrument and therefore would appear as a loss of total amplitude. A strong possibility is that prolonged exposure to 1.0 M NaSCN leads to oxidative damage of the intersubunit F_X [4Fe-4S] cluster. This conclusion is supported by trEPR studies of membranes after treatment with 2.0 M NaSCN, which show a spin-polarized triplet from charge recombination between A_0^- and $P840^+$ (see Fig. 9c and accompanying text below).

The charge recombination kinetics of chlorosome-depleted *C. thermophilum* membranes measured by EPR under anoxic conditions at 90 K is depicted in Fig. S2. The amplitude of the high-field peak of the P_{840}^+ radical at ~g = 2 was recorded as a function of time after a laser flash. The data can be fit as a mono-exponential decay with a lifetime of ~80 ms. By analogy with *Cba. tepidum* RCs, for which electron transfer from F_X^- to F_A/F_B is inefficient at temperatures <200 K (Jaganathan and Golbeck, 2008), this charge recombination event can be assigned to $P_{840}^+ F_X^-$. Hence, the recombination between F_X^- and P_{840}^+ slows marginally from 20-30 ms at room temperature to 80 ms at 90 K.

Properties of the bound FeS clusters in *C. thermophilum*

We were unable to obtain a CW-EPR spectrum of the reduced F_X cluster in *C. thermophilum* using field modulation due to limitations of sample concentration and volume. However, we were able to determine the midpoint potential of F_X by titrating the trEPR signal of the spin-correlated $P^+ F_X^-$ radical pair against solution potential. The trEPR-detected radical pair spectra of PBS-washed membranes poised at different solution potentials is shown in Fig. 7a. As the solution potential is lowered from –283 mV to –592 mV, the amplitude of the radical-pair signal diminishes. When the amplitude of the absorptive feature of the radical-pair spectrum is plotted against solution potential, and the data are fitted using the Nernst equation with *n*

= 1 (Fig. 7b), the midpoint potential of F_X is found to be –581 ± 7 mV versus the SHE. This value is 77 mV more reducing than the –504 ± 10 mV midpoint potential measured for F_X in RCs from *H. modesticaldum* (Ferlez et al., 2016) but is only 29 mV more oxidizing than the –610 mV midpoint potential measured for F_X in cyanobacterial PSI in the absence of PsaC (Parrett et al., 1989; Ishikita et al., 2006).

The trEPR spectra at 90 K of the spin-polarized radical pair in whole cells of representatives of the three phyla that contain homodimeric Type-1 RCs: *H. modesticaldum* (*Firmicutes*), *Chlorobaculum* (*Cba.*) *parvum* (*Chlorobi;* a close relative of *Cba. tepidum*), and *C. thermophilum* (*Acidobacteria*) are compared in Fig. S3a. When the radical-pair spectra are normalized and overlaid (Fig. S3b), all three Type-1 RCs show a highly similar, spin-polarized emissive-absorptive (E-A) pattern with a net absorption, and with an emissive feature at 345.3 mT and an absorptive feature at 346.1 mT. Similar to the other homodimeric Type-1RCs, *C. thermophilum* RCs show no evidence for the participation of a $P^+ A_1^-$ radical pair in either forward or backward electron transfer (van der Est et al., 1998). Instead, the spectrum is diagnostic of a spin-polarized $P^+ F_X^-$ radical pair, implying that electron transfer occurs directly from A_0^- to F_X in all homodimeric Type-1 RCs.

The field-modulated CW-EPR spectrum of the F_A/F_B clusters *C. thermophilum* RCs is shown in Fig. 8. When the sample was frozen in the dark and measured at 17 K, a large resonance with axial symmetry was recorded with a *g*-value around 2.03 characteristic of a $[3Fe\text{-}4S]^{1+}$ cluster (data not shown). When the sample was illuminated at 17 K, an additional set of resonances appeared with rhombic symmetry and *g*-values of 2.06, 1.94 and 1.91 characteristic of a reduced iron-sulfur cluster (Fig. 8, black trace, dark signal subtracted). Note that the resonance at $g = 2.03$ from the $[3Fe\text{-}4S]^{1+}$ cluster is still present, but because this is a light-minus-dark difference spectrum, it appears inverted. When the light was turned off, the amplitude of the rhombic set of resonances diminished by about 50%, (red trace, dark signal subtracted), indicating that the charge separation was only partly reversible at low temperature. The $g = 2.03$ resonance also appeared to diminish after the light was turned off; the reasons for this are unclear. When the sample was thawed, frozen slowly during illumination, and then measured in the dark, an 'interaction' spectrum appeared, which showed a complex set of resonances from 335 mT to 370 mT characteristic of two spin-

coupled iron-sulfur clusters (data not shown). This process, termed photoaccumulation, leads to the irreversible accumulation of two electrons in the acceptor system, one each in F_A and F_B. It is presently uncertain whether the F_A/F_B clusters *C. thermophilum* RCs are sensitive to prolonged exposure to oxygen or whether the observed [3Fe-4S] cluster is a result of the sensitivity of PscB to proteolysis, or both. Additional studies will be required with membranes isolated under anoxic conditions and at higher concentrations to determine more accurately the properties of the F_A and F_B clusters.

Spin-polarized EPR triplet signals from radical pair recombination

When PBS-washed membranes were measured by trEPR over a wide field range of 310 mT to 380 mT, the as-isolated membranes showed, in addition to the ~4 mT-wide, spin-polarized $P^+F_X^-$ radical pair signal, an additional ~60 mT wide, minor signal with an E/E/E/A/A/A polarization pattern characteristic of a triplet from BChl *a* antenna molecules as a result of intersystem crossing (Fig. 9a, red trace) (Monger et al., 1976). The low amplitude of this signal indicates that most of the antenna excited states are effectively trapped by P_{840}. When the same membranes were reduced with sodium dithionite at pH 10.0 to reduce the F_X cluster (see Fig. 7), the resulting EPR spectrum showed an intense ~60 mT wide, spin-polarized triplet signal with an A/E/E/A/A/E polarization pattern characteristic of $P^+A_0^-$ radical pair recombination as a result of singlet-triplet mixing (Thurnauer et al., 1975) in the primary radical pair (Fig. 9a, black trace). The zero field splitting parameters were extracted by measuring the width of characteristic features of the first derivative spectrum (Fig. 9b). The values of $D = 208 \times 10^{-4}$ cm^{-2} and $E = 35 \times 10^{-4}$ cm^{-2} are similar to those found for the spin-polarized triplet from $P^+A_0^-$ radical pair recombination in *Cba. tepidum* of $D = 208 \times 10^{-4}$ cm^{-2} and $E = 32/33 \times 10^{-4}$ cm^{-2} (Table 1) (van der Est et al., 1998; Ferlez et al., 2017). This correspondence is expected, as the primary electron acceptor is a chlorin (Chl *a*) and the primary electron donor is a bacteriochlorin (BChl *a* or Zn-BChl *a'*) in both *Cba. tepidum* and *C. thermophilum* (Zill et al., 2018; Charles et al., 2019). In contrast, the absence of a spin-polarized triplet from $P^+A_0^-$ radical pair recombination in *H. modesticaldum* is a result of the fact that the primary electron donor is BChl *g*. Because of the D and E

values, the zero-field splitting (ZFS) tensor of $^3P_{800}$ is maximally rhombic, which results in complete cancelation of the absorptive and emissive polarization in a randomly oriented sample (Ferlez et al., 2017).

The trEPR spectrum of *C. thermophilum* membranes after treatment with 2.0 M sodium thiocyanate is shown in Fig. 9c. The intense spin-polarized triplet signal with an A/E/E/A/A/E polarization pattern is identical to that of Fig. 9a, and thus is derived from $P^+ A_0^-$ radical pair recombination. This supports the result of the transient absorbance study described above (see Fig. 6d and accompanying text). We therefore suggest that the reduction in the signal amplitude by transient optical absorption spectroscopy is due to the destruction of the F_X cluster when membranes were treated with 1.0 M sodium thiocyanate for 1 h.

Discussion

Type-1 RCs have [4Fe-4S] clusters as terminal electron acceptors, and as a consequence produce a strong reductant and a weak oxidant (P_{840}^+) when illuminated (Golbeck, 1993). As a result, these RCs can sometimes reduce dioxygen to produce reactive oxygen species or the [4Fe-4S] clusters can be damaged and inactivated by oxygen. Until very recently, homodimeric type-1 RCs were only known to occur in members of the *Heliobacteriaceae* (*Firmicutes*) and the *Chlorobiaceae* (*Chlorobi*), all of which are strict anaerobes. The discoveries of *C. thermophilum* (Bryant et al., 2007) and "*Ca*. T. aerophilum" (Liu et al., 2012; Tank et al., 2017) demonstrated that homodimeric type-1 RCs could be adapted through evolution to tolerate oxygen, but to what extent and how was unknown. Thus, from evolutionary and mechanistic perspectives, it was of interest to know how inherently oxygen-sensitive, ancestral RCs might have been modified to produce the heterodimeric, oxygen-tolerant RCs of cyanobacteria.

C. thermophilum is currently the only microaerophile (or aerobe) with type-1 homodimeric RCs that is available in pure culture (Tank and Bryant, 2015a, b; Tank et al., 2018). The only other known aerobe with homodimeric type-1 RCs is "*Ca*. T. aerophilum" (Liu et al., 2012; Tank et al., 2017; Thiel et al., 2018). However, "*Ca*. T. aerophilum" has only been grown to date in enrichment cultures, and thus its RCs have not yet been characterized in detail. Previous studies showed that the primary electron acceptor in all characterized type-1 RCs is a chlorin molecule. Heliobacterial RCs employ 8^1-OH-Chl *a* as the primary

electron acceptor (van de Meent et al., 1991), and green sulfur bacteria (van de Meent et al., 1992) and PSI (Shuvalov et al., 1979; Mathis et al., 1988) have Chl a_{PD} and Chl a_P, respectively, as the primary electron acceptor (spectroscopically denoted as A_0). These two molecules only differ in the number of double bounds in the esterifying alcohol group associated with the chlorin macrocyle (Gomez Maqueo Chew and Bryant, 2007). Because we are interested in deciphering how type-1 RCs adapted during evolution to cope with current atmospheric oxygen levels, we sought to characterize the RCs of *C. thermophilum* in greater detail. In previously characterized homodimeric RCs, either the 13^1-epimer of BChl *g* (heliobacteria) or the equivalent epimer of BChl *a* (green sulfur bacteria) is used to form the primary electron donor (special pair) electron donor. In the heterodimeric type-1 RC in cyanobacteria, the P700 special pair is formed from one Chl a_P molecule and one Chl a_P' molecule. Thus, it seemed highly probable that two Zn-BChl a_P' molecules would form the special pair in the RCs of *C. thermophilum*. The studies described herein were undertaken to answer these and other questions concerning the properties of these RCs. The studies in an accompanying study (Charles et al., 2019) by ^{67}Zn-HYSCORE spectroscopy of $P840^+$ have established that the special pair is indeed formed from Zn-BChl a_P'.

The *pscA-pscB-fmoA* operon, which encodes the RC core proteins and FMO, contains three additional open reading frames (ORFs) (Cabther_A2185, Cabther_A2184, and Cabther_A2183) (see Fig. 2e) (Bryant et al., 2007; Garcia Costas et al., 2012). The function of the ArsA-like ATPase encoded by Cabther_A2185 is unknown, and this protein was not detected in any of the RC preparations described in this study. The other two open reading frames in the operon are predicted to encode membrane-intrinsic, monoheme *c*-type cytochromes. The copurification of these two cytochromes with PscA in moderately and highly purified RC preparations strongly suggests that these two cytochromes play a role in RC function, probably as secondary electron donors to P_{840}^+. The sequences of both ORFs predict that these cytochromes are lipoproteins, which should be acylated on an N-terminal cysteine residue, which would be revealed after transfer of the heme-binding domain to the periplasm and subsequent cleavage of the signal peptides. The role of these two cytochromes in RC function was not addressed in this study and will require further investigation in future studies. Based upon the pigment content of our most highly purified RC fractions

that were totally devoid of FMO, and assuming that the RCs contain 60 BChls like the reaction center of *H. modesticaldum*, we estimate that the *C. thermophilum* RCs should contain 4 Zn-BChl a_P', 32 BChl a_P, 22 Chl $a_{PD,}$ and ~2 Chl a_P molecules. Unfortunately, complete removal of FMO also caused complete loss of PscB. PscB also appeared to be sensitive to proteolytic degradation, which makes it difficult to study the terminal electron acceptors associated with this protein.

The high-resolution, light-induced difference spectrum for P_{840}^+ reported here for RCs from *C. thermophilum* establishes that the maximal photobleaching of the special pair, P^+, actually occurs at ~839 nm. For convenience and consistency with other literature, we nonetheless will continue to refer to the special pair as P840, as the bleaching is nearly equivalent over a few nanometers near this wavelength. Because a much higher resolution was obtained in this study than in our previous one (Tsukatani et al., 2012), it is also possible to see a probable electrochromic bandshift in the difference spectrum that reflects the effect of the electric charge of P_{840}^+ on nearby RC pigments. These spectral changes occur between 790 nm and 830 nm, and for this reason, it is highly unlikely that they emanate from Chl a_{PD}, and therefore, they must logically be due to changes in the absorbance of bacteriochlorin molecules in the accessory (A_{-1}) position in the electron transport chain. Thus, this electrochromic bandshift could either be derived from BChl a_P or from the two remaining molecules of Zn-BChl a_P'. However, if the RC of *C. thermophilum* has epimeric forms of BChl a_P among the antenna pigments of the RC, as occurs in the RCs of *H. modesticaldum* (Gisriel et al., 2017), then the accessory (A_{-1}) position in the electron transport chain would then be occupied by BChl a_P. Because of the similar absorption properties of BChl a_P and Zn-BChl a_P', it is currently not possible to distinguish between these two possibilities. Overall, the electron transfer chain components associated with PscA of *C. thermophilum* RCs would comprise a dimer of Zn-BChl a_P' (P_{840}) (see Charles et al., 2019), probably 2 Mg-BChl a_P (A_{-1}), 2 Chl a_{PD} molecules (A_0) (Zill et al., 2018), and the intersubunit F_X [4Fe-4S] cluster. The arrangement of these pigments is shown in Fig. 10.

The issue of whether there is a quinone in type-1 RCs that is functionally equivalent to phylloquinone A_1 of PSI has been controversial for many years (Oh-Oka 2007; Heinnickel and Golbeck, 2007). The X-ray crystal structure of the *H. modesticaldum* RC indicates that no quinone exists in the same

position as one exists in PSI (Gisriel et al., 2017). The trEPR studies demonstrate that charge separation (or charge recombination) in the RCs of *C. thermophilum* occurs directly between P840 and F_X without the participation of an intermediary quinone. The spectra of spin-polarized radical pairs, $P^+F_X^-$, were essentially identical for representatives of type-1 RCs from each of the three phyla with this type of RC (Fig. S3). Whether there is a quinone or not, these results demonstrate that charge separation and recombination pathways are very similar in all homodimeric type-1 RCs, and that they differ from those of heterodimeric PSI RCs. However, the redox properties of the F_X [4Fe-4S] cluster of the RC of *C. thermophilum* differ slightly from those of other organisms with type-1 RCs. The F_X cluster in cyanobacterial PSI is the most reducing, with a midpoint potential of –610 mV (Parrett et al., 1989; Ishikita et al., 2006), and that of *H. modesticaldum* has the highest midpoint potential, which is about 100 mV less reducing (–504 mV) (Ferlez et al., 2016). The midpoint potential of F_X in green sulfur bacterial RCs has not been directly measured, but on the basis of flash-induced recombination kinetics for *Cba. tepidum* RCs, the midpoint potential of F_X has been suggested to be about 60 mV more reducing than the potential of Fe/S cluster I (Sétif et al., 2001). Studies with the RCs of *Chlorobium vibrioforme* (now *Chlorobaculum parvum*) indicate that the midpoint potentials of centers I and II of PscB are approximately –446 mV and –501 mV (Scott et al., 1997). Together, these findings suggest that the midpoint potential of F_X in green sulfur bacterial RCs is similar to that of *H. modesticaldum* RCs, approximately –506 mV. The midpoint potential determined here for the F_X cluster in *C. thermophilum* RCs was –581 mV, which is nearly as reducing as the F_X cluster in cyanobacterial PSI. Whether this reflects an important functional adaptation to microoxic growth conditions is uncertain, but the observed trend suggests that it might be significant. The reduction potential of F_X must necessarily be sufficiently reducing to reduce the Fe/S clusters in PscB efficiently, and thus the midpoint potential(s) of the clusters in the PscB (or PsaC in PSI) and the redox state of the ferredoxin pool in cells could ultimately determine the midpoint potential range for F_X.

In the RCs of *H. modesticaldum*, the PshB protein is loosely bound to the RC (Heinnickel et al., 2005, 2007; Heinnickel and Golbeck, 2007; Romberger et al., 2010). This situation is functionally possible for strict anaerobes, such as *H. modesticaldum* or green sulfur bacteria like *Cba. tepidum*, which rarely

encounter oxygen in their growth habitats. The possibility of oxygen being reduced by a reduced PscB/PshB protein is unlikely for a strict anaerobe. However, *C. thermophilum* is a microaerophile and requires some oxygen for some important biochemical reactions, including Chl and tyrosine biosynthesis, essential functions for an obligate phototroph. One of us has suggested that an important event in the evolutionary transition from homodimeric RCs with transiently or weakly bound PscB proteins would have been the gene duplication to form the heterodimeric core complex (Jaganathan and Golbeck, 2008). This would thereby have allowed the PsaC protein, the functional equivalent of PscB, to become permanently bound to the RC core complex through its interactions with the PsaD "clamping" subunit. PsaD has no symmetry elements, thereby requiring the differentiation of a homodimeric RC into a heterodimeric RC. The backreaction kinetics for P_{840}^{+} in membranes subjected to different wash treatments indicate that PscB from *C. thermophilum* is much more tightly associated with PscA than PshB1 and PshB2 are with PshA. Thus, the interaction of PscB with PscA in the RCs of *C. thermophilum* is more similar to the situation in cyanobacterial PSI than to the situation in *H. modesticaldum*. A more tightly bound PscB protein could help to preclude oxygen from interacting with the strongly reducing F_X and F_A clusters of the *C. thermophilum* RC.

In conclusion, in this study we have characterized the homodimeric type-1 RCs of the microaerophilic anoxygenic chlorophototroph, *C. thermophilum*. Our studies show that these RCs are similar in overall properties to homodimeric type-1 RCs of strict anaerobes in several respects, but nevertheless have some properties that might help to protect the RCs from the damaging effects of oxygen. At this time, it is not known why nature has elected to utilize Zn-BChl a_P' as the primary electron donor, P840. The *C. thermophilum* RCs are the first to contain three types of (B)Chl. These RCs are also the first to contain large pools of both Chl *a* and BChl *a*, which would allow these RCs to absorb both visible and near-infrared light efficiently. In future studies it will be interesting to determine how these pigments are arranged so as to avoid low-energy wells in the core antenna region that might reduce the efficiency of charge separation.

Acknowledgements

The authors thank Dr. Tatiana N. Laremore of the Proteomics and Mass Spectrometry core facility (Huck Institutes for the Life Sciences, The Pennsylvania State University) for performing the tryptic peptide fingerprinting studies reported here. Studies in the laboratories of D.A.B. and J.H.G. were supported by grants DE-FG02-94ER20137 and DE-SC0010575, respectively, from the Photosynthetic Systems Program, Division of Chemical Sciences, Geosciences, and Biosciences (CSGB), Office of Basic Energy Sciences of the U. S. Department of Energy.

Conflict of Interest Statement

The authors declare that the research was conducted in the absence of any commercial or financial relationships that could be construed as a potential conflict of interest.

References

Blum H, Beier H, Gross HJ (1987) Improved silver staining of plant proteins, RNA and DNA in polyacrylamide gels. Electrophoresis 8:93–99

Bryant DA (1994) *The Molecular Biology of Cyanobacteria*. *Advances in Photosynthesis and Respiration*, Vol 1. Springer, Dordrecht, The Netherlands.

Bryant DA, Frigaard NU (2006) Prokaryotic photosynthesis and phototrophy illuminated. Trends Microbiol 14:488–496

Bryant DA, Garcia Costas AM, Maresca JA, Chew AGM, Klatt CG, Bateson MM, Tallon LJ, Hostetler J, Nelson WC, Heidelberg JF, Ward DM (2007) *Candidatus* Chloracidobacterium thermophilum: an aerobic phototrophic acidobacterium. Science 317:523–526

Cardona T, Murray JW, Rutherford AW (2015) Origin and evolution of water oxidation before the last common ancestor of the cyanobacteria. Mol Biol Evol 32:1310–1328

Charles P, Kalendra V, He, Z, Khurshov, V, van der Est A, Golbeck JH, Bryant, DA, and Lakshmi KV 2018. Elucidating the role of zing-bacteriochlorophyll *a′* in the primary photochemistry of *Chloracidobacterium thermophilum* reaction centers. Biophys J 116:419a

van der Est A, Hager-Braun C, Leibl W, Hauska G, Stehlik D (1998) Transient electron paramagnetic resonance spectroscopy on green-sulfur bacteria and heliobacteria at two microwave frequencies, Biochim Biophys Acta 1409:87–98

Ferlez B, Agostini A, Carbonera D, Golbeck JH, van der Est A (2017) Triplet charge recombination in heliobacterial reaction centers does not produce a spin-polarized EPR spectrum. Z Phys Chem 231:593–607

Ferlez B, Cowgill J, Dong W, Gisriel C, Lin S, Flores M, Walters K, Cetnar D, Redding KE, Golbeck JH (2016) Thermodynamics of the electron acceptors in *Heliobacterium modesticaldum*: an exemplar of an early homodimeric type I photosynthetic reaction center. Biochemistry 55:2358–2370

Frigaard N-U, Takaichi S, Hirota M, Shimada K, Matsuura K (1997) Quinones in chlorosomes of green sulfur bacteria and their role in the redox-dependent fluorescence studied in chlorosome-like bacteriochlorophyll *c* aggregates. Arch Microbiol 167:343–349

Grotjohann I, Fromme P (2005) Structure of cyanobacterial photosystem I. Photosynth Res 85:51–72

Garcia Costas AM, Tsukatani Y, Romberger SP, Oostergetel G, Boekema E, Golbeck JH, Bryant DA (2011) Ultrastructural analysis and identification of envelope proteins of "*Candidatus* Chloracidobacterium thermophilum" chlorosomes. J Bacteriol 193:6701–6711

Garcia Costas AM, Liu Z, Tomsho LP, Schuster SC, Ward DM, Bryant DA (2012) Complete genome of *Candidatus* Chloracidobacterium thermophilum, a chlorophyll-based photoheterotroph belonging to the phylum Acidobacteria. Environ Microbiol 14:177–190

Garcia Costas AM, Tsukatani Y, Rijpstra WIC, Schouten S, Welander PV, Summons RE, Bryant DA (2012) Identification of the bacteriochlorophylls, carotenoids, quinones, lipids, and hopanoids of "*Candidatus* Chloracidobacterium thermophilum." J Bacteriol 194:1158–1168

Gisriel C, Sarrou I, Ferlez B, Golbeck JH, Redding KE, Fromme R (2017) Structure of a symmetric photosynthetic reaction center-photosystem. Science 357:1021–1025

Golbeck JH (1993) Shared thematic elements in photochemical reaction centers. Proc Natl Acad Sci USA 90:1642–1646

Golbeck JH, Bryant DA (1991) Photosystem I. In: *Current Topics in Bioenergetics: Light-Driven Reactions in Bioenergetics* (Lee CP, ed), Academic Press, New York, pp 83-177.

Gomez Maqueo Chew A, Bryant DA (2007) Chlorophyll biosynthesis in bacteria: the origins of structural and functional diversity. Annu Rev Microbiol 61:113–129

Heinnickel M, Golbeck JH (2007) Heliobacterial photosynthesis. Photosynth Res 92:35–53

Heinnickel M, Shen G, Agalarov R, Golbeck JH (2005) Resolution and reconstitution of a bound Fe-S protein from the photosynthetic reaction center of *Heliobacterium modesticaldum*. Biochemistry 44:9950–9960

Heinnickel M, Shen G, Golbeck JH (2007) Identification and characterization of PshB, the dicluster ferredoxin that harbors the terminal electron acceptors F(A) and F(B) in *Heliobacterium modesticaldum*. *Biochemistry* 46:2530–2536

Hiyama T, Ke B (1972) Difference spectra and extinction coefficients of P700. Biochim Biophys Acta 267:160–171

Ishikita H, Stehlik D, Golbeck JH, Knapp EW (2006) Electrostatic influence of PsaC protein binding to the PsaA/PsaB heterodimer in Photosystem I. Biophys J 90:1081–1089

Jagannathan B, Golbeck JH (2008) Unifying principles in homodimeric type I photosynthetic reaction centers: properties of PscB and the F_A, F_B and F_X iron-sulfur clusters in green sulfur bacteria. Biochim Biophys Acta 1777:1535–1544

Jordan P, Fromme P, Witt HT, Klukas O, Saenger W, Krauss N (2001) Three-dimensional structure of cyanobacterial photosystem I at 2.5Å resolution. Nature 411:909–917

Klatt CG, Wood JM, Rusch DB, Bateson MM, Hamamura N, Heidelberg JF, Grossman AR, Bhaya D, Cohan FM, Kühl M, Bryant DA, Ward DM (2011) Community ecology of hot spring cyanobacterial mats: predominant populations and their functional potential. ISME J 5:1262–1278

Liu Z, Klatt CG, Ludwig M, Rusch DB, Jensen SI, Kühl M, Ward DM, Bryant DA (2012) '*Candidatus Thermochlorobacter aerophilum*:' an aerobic chlorophotoheterotrophic member of the phylum *Chlorobi* defined by metagenomics and metatranscriptomics. ISME J 6:1869–1882

Mathis P, Ikegam I, Sétif P (1988) Nanosecond flash studies of the absorption spectrum of the photosystem I primary acceptor A_0. Photosynth Res 16:203–210

van de Meent EJ, Kobayashi M, Erkelens C, van Veelen PA, Amesz J, Watanabe T (1991) Identification of 8^1-hydroxychlorophyll *a* as a functional reaction center pigment in heliobacteria. Biochim Biophys Acta 1058:356–362

van de Meent EJ, Kobayashi M, Erkelens C, van Veelen PA, Otte S, Inoue K, Watanabe T, Amesz J (1992) The nature of the primary electron acceptor in green sulfur bacteria. Biochim Biophys Acta 1102:371–378

Monger TG, Cogdell RJ, Parson WW (1976) Triplet states of bacteriochlorophyll and carotenoids in chromatophores of photosynthetic bacteria. Biochim Biophys Acta 449:136-153

Nitschke W, Rutherford AW (1991) Photosynthetic reaction centres: variations on a common structural theme? Trend Biochem Sci 16:241–245

Oh-oka H (2007) Type 1 reaction center of photosynthetic heliobacteria. Photochem Photobiol 83:177–186

Parrett KG, Mehari T, Warren PG, Golbeck JH (1989) Purification and properties of the intact P-700 and Fx-containing photosystem I core protein, Biochim Biophys Acta 973:324–332

Romberger SP, Castro C, Sun Y, Golbeck JH (2010) Identification and characterization of PshBII, a second F_A/F_B-containing polypeptide in the photosynthetic reaction center or *Heliobacterium modesticaldum*. Photosynth Res 104:293–303

Sadekar S, Raymond J, Blankenship RE (2006) Conservation of distantly related membrane proteins: photosynthetic reaction centers share a common structural core. Mol Biol Evol 23:2001–2007

Schaffernicht H, Junge W (1981) Analysis of the complex band spectrum of P700 based on photoselection studies with photosystem I particles, Photochem Photobiol 34:223–232

Scott MP, Kjær B, SchellerShen G, Bryant DA (1995) Characterization of a *Synechococcus* sp. strain PCC 7002 mutant lacking photosystem I. Protein assembly and energy distribution in the absence of the photosystem I reaction center core complex. Photosynth Res 44:41–53

Shen, J.-R. (2015) The structure of photosystem II and the mechanism of water oxidation in photosynthesis. Annu Rev Plant Biol 66:23–48

Shuvalov VA, Klevanik AV, Sharkov AV, Kryukov PG, Ke B (1979) Picosecond spectroscopy of photosystem I reaction centers. FEBS Lett 107:313–316

Tank M, Bryant DA (2015a) *Chloracidobacterium thermophilum* gen. nov., sp. nov.: an anoxygenic microaerophilic chlorophotoheterotrophic acidobacterium. Int J Syst Evol Microbiol 65:1426–1430

Tank M, Bryant DA (2015b) Nutrient requirements and growth physiology of the photoheterotrophic Acidobacterium, *Chloracidobacterium thermophilum*. Front Microbiol 6:226

Tank M, Thiel V, Ward DM, Bryant DA (2017) A panoply of phototrophs: an overview of chlorophototrophs found in the microbial mats of alkaline siliceous hot springs in Yellowstone National Park, WY, USA. In: *Modern Topics in the Phototrophic Prokaryotes: Environmental and Applied Aspects*, (Hallenbeck PC, ed.), Springer, Berlin, pp 87–137

Tank M, Garcia Costas AM, Bryant DA (2018) Genus: *Chloracidobacterium*. In: *Bergey's Manual of Systematics of Bacteria and Archaea* (W. B. Whitman, supervising editor), Wiley, New York.

Thiel V, Tank M, Bryant DA (2018) Diversity of chlorophototrophic bacteria revealed in the omics era. Annu Rev Plant Biol 69:21–49

Thurnauer MC, Katz JJ, Norris JR (1975) The triplet state in bacterial photosynthesis: Possible mechanisms of the primary photo-act. Proc Natl Acad Sci USA 72:3270–3274

Thweatt JL, Canniffe DP, Bryant DA (2019) Biosynthesis of chlorophylls and bacteriochlorophylls in green bacteria. In *Advances in Botanical Research*, Vol. 90, *Metabolism, structure and function of chlorophylls*, (B Grimm, ed), in press, Elsevier, Amsterdam

Tomi T, Shibata Y, Ikeda Y, Taniguchi S, Haik C, Mataga N, Shimada K, Itoh S. 2007. Energy and electron transfer in the photosynthetic reaction center complex of *Acidiphilium rubrum* containing Zn-bacteriochlorophyll *a* studied by femtosecond up-conversion spectroscopy. Biochim Biophys Acta 1767:22–30

Tsukatani Y, Wen J, Blankenship RE, Bryant DA (2010) Characterization of the bacteriochlorophyll *a*-binding, Fenna-Matthews-Olson protein from *Candidatus* Chloracidobacterium thermophilum. Photosynth Res 104:201–209

Tsukatani Y, Romberger SP, Golbeck JH, Bryant DA (2012) Isolation and characterization of homodimeric type-I reaction center complex from Candidatus *Chloracidobacterium thermophilum*, an aerobic chlorophototroph. J Biol Chem 287:5720–5732

Vassiliev IR, Jung YS, Mamedov MD, Semenov A, Golbeck JH (1997) Near-IR absorbance changes and electrogenic reactions in the microsecond-to-second time domain in Photosystem I. Biophys J 72:301–315

Wakao N, Yokoi N, Isoyama N, Hiraishi A, Shimada K, Kobayashi M, Kise H, Iwaki M, Itoh S, Takaichi S (1996) Discovery of natural photosynthesis using Zn-containing bacteriochlorophyll in an aerobic bacterium *Acidiphilium rubrum*. Plant Cell Physiol 37:889–893

Ward LM, McGlynn SE, Fischer WW (2017) Draft genome sequence of *Chloracidobacterium* sp. CP2_5A, a phototrophic member of the phylum *Acidobacteria* recovered from a Japanese hot spring. Genome Announc 5:300821-17

Wen J, Tsukatani Y, Cui W, Zhang H, Gross ML, Bryant DA, Blankenship RE (2011) Structural model and spectroscopic characteristics of the FMO antenna protein from the aerobic chlorophototroph, *Candidatus* Chloracidobacterium thermophilum. Biochim Biophys Acta 1807:157–164

Zeng Y, Feng F, Medova H, Dean J, Koblížek M (2014) Functional type 2 photosynthetic reaction centers found in the rare bacterial phylum *Gemmatimonadetes*. Proc Natl Acad Sci USA 111:7795–7800

Zill JC, He Z, Tank M, Ferlez BH, Canniffe DP, Lahav Y, Bellstedt P, Alia A, Schapiro I, Golbeck JH, Bryant DA, Matysik J (2018) ^{15}N photo-CIDNP MAS NMR analysis of reaction centers of *Chloracidobacterium thermophilum*. Photosynth Res 137:295-305

Table 1. Zero-field splitting parameters for the spin-polarized triplet produced by P^+ A_0^- radical-pair recombination in *C. thermophilum* and *Cba. tepidum.*

Zero Field Splitting Parameters	*C. thermophilum*[a] 90 K ($\times 10^{-4}$ cm^{-1})	*Cba. tepidum*[b] 90 K ($\times 10^{-4}$ cm^{-1})	*Cba. tepidum*[c] 80 K ($\times 10^{-4}$ cm^{-1})
D	208	208	208
E	35	32	33

[a]This study
[b]Ferlez et al., 2017
[c]van der Est et al., 1998

Figure Legends

Fig. 1 Isolation of crude *C. thermophilum* RCs by sucrose gradient centrifugation. a Separation of crude RCs from PBS-washed membranes (see Fig. S1) on a 5 to 25% linear sucrose gradient after solubilization with 1% (w/v) DM. The grayish-brown RC fraction is well separated from the bright orange fraction containing the carotenoid binding protein, CbpA. **b** SDS-PAGE analysis of the crude RC preparation (gel was stained with Coomassie blue). This preparation retained some PscB and but contained a number of contaminating proteins (e.g., FMO). **c** Absorbance spectrum of crude RCs isolated by sucrose gradient centrifugation. The numbers on the right indicate the polypeptide bands excised and subjected to tryptic peptide mass fingerprinting (see Table S1). Four polypeptides encoded within the *pscA* operon (see Fig. 2e) are also identified.

Fig. 2 Preparation of highly purified RCs from *C. thermophilum*. First (**a**) and second (**b**) linear 5 to 25% sucrose gradients used to prepare a crude RC fraction devoid of the carotenoid-binding protein CbpA. The blue arrowheads identify the RC complexes. The crude RCs were further purified by chromatography on DEAE-cellulose (see Materials and Methods) and were analyzed on SDS-PAGE gels stained with Coomassie blue (**c**) or silver (**d**). Markers and their sizes are shown to the left, and selected proteins are identified by the locus tag numbers for the corresponding genes. Panel **e** shows the organization of the reaction center operon that includes *pscA*, *pscB*, and *fmoA* as well as a gene encoding an ArsA-like ATPase and two predicted *c*-type cytochrome lipoproteins.

Fig. 3 Absorbance spectrum of highly purified *C. thermophilum* RCs that are devoid of FMO.

Fig. 4 Reversed-phase HPLC analysis of the pigments in a preparation of *C. thermophilum* RCs that was devoid of FMO contamination. The elution profiles for 770 nm (BChl *a*; black line) and 665 nm (Chl *a*; red line) are shown with a slight offset for clarity. The very minor peaks eluting at 35 to 37 minutes had absorption spectra similar to BChl *a* and may represent BChl *a* with less reduced esterifying alcohol tails

(see text). The (B)Chl species were identified by their elution times compared to standards, their absorption spectra, and by mass spectral analysis of each peak fraction.

Fig. 5 High-resolution light-induced difference spectrum of P_{840}^+ in isolated RCs of *C. thermophilum.* The RC samples used for this analysis isolated by sucrose gradient ultracentrifugation as shown in Fig. 1 (and with no DEAE-cellulose chromatography step; see text). The difference spectrum was measured by continuous illumination at room temperature in the presence of 10 mM sodium ascorbate. The insert shows the region between 820 nm and 850 nm in greater detail.

Fig. 6 Charge recombination kinetics of chlorosome-depleted *C. thermophilum* membranes measured at 840 nm after a laser flash. a Control sample measured under anoxic conditions in the presence of 30 mM sodium ascorbate as the immediate electron donor to P_{840}^+. **b** After treatment with 500 mM NaCl and 100 mM sodium carbonate. **c** After 30-min exposure to 1.0 M NaSCN. **d** After 1-h exposure to 1.0 M NaSCN. Multi-exponential decay curves (red lines) were fitted to the data (blue circles) and the residuals of the fit are displayed above each plot.

Fig. 7 Determination of the midpoint potential of the F_X cluster by trEPR. a Representative trEPR-detected radical pair spectra of PBS-washed membranes of *C. thermophilum* poised at different solution potentials. **b** Redox titration of the absorptive feature of the radical pair signal. For additional details, see text.

Fig. 8 CW EPR spectrum of isolated RCs from *C. thermophilum*. The sample was frozen in the dark and illuminated at 17 K. The light-minus dark difference spectrum is shown as the black trace and after subsequent darkness (minus the dark spectrum) as the red trace. Note the presence of the inverted $g = 2.03$ radical attributed to a $[3Fe\text{-}4S]^{1+}$ cluster in the difference spectrum. Measurement conditions: Temperature, 17 K; microwave power, 80 mW (4 dB); modulation amplitude, 2 mT; average of 4 scans.

Fig. 9 TrEPR spectra of chlorosome depleted membranes collected in direct detection mode. a TrEPR spectra of as-isolated chlorosome depleted membranes (red trace) and the same after reduction with sodium dithionite at pH 10.0 (black trace). **b** Extraction of zero field splitting parameters D and E from the charge recombination $^{T}P_{840}$ observed in chemically reduced chlorosome-depleted membranes (gray solid line) from (**a**) by measuring the width of the features of its first derivative (dashed red line). See Table 1 for extracted D and E values. **c** Charge recombination triplet of P_{840} at 90 K as measured by trEPR in *C. thermophilum* membranes treated with 2 M NaSCN. The spectra were collected in direct detection mode and the box car spectra shown represent the integrated signal of the 3D time-field-amplitude data sets between 1-2 μsec following the ~20 mJ/pulse of light at 532 nm provided by a frequency doubled Nd:YAG laser. Field resolution was 0.5 mT and 160 transients were averaged per field position.

Fig. 10 Arrangement of the electron transport chain cofactors in the RCs of *C. thermophilum*. This model is based on the position of the cofactors in the structure of the *H. modesticaldum* homodimeric type-1 RC (PDB entry 5VHK; Gisriel et al., 2017). The electron transport chain comprises a P840 dimer of Zn-BChl a_P' molecules (Charles et al., 2019); the accessory Chls A_{-1}, which are most likely Mg-BChl a_P (or possibly Zn-BChl a_P'; see text); and the primary acceptor Chls, A_0, which are Chl a_{PD} (Zill et al., 2018). Zn^{2+} ions are shown as gray spheres, and Mg^{2+} ions are shown as green spheres. The intrasubunit [4Fe-4S] cluster F_X is ligated by two cysteine residues from each PscA subunit of the RC homodimer. The esterifying alcohol tail groups have been omitted for clarity.

Figure 1

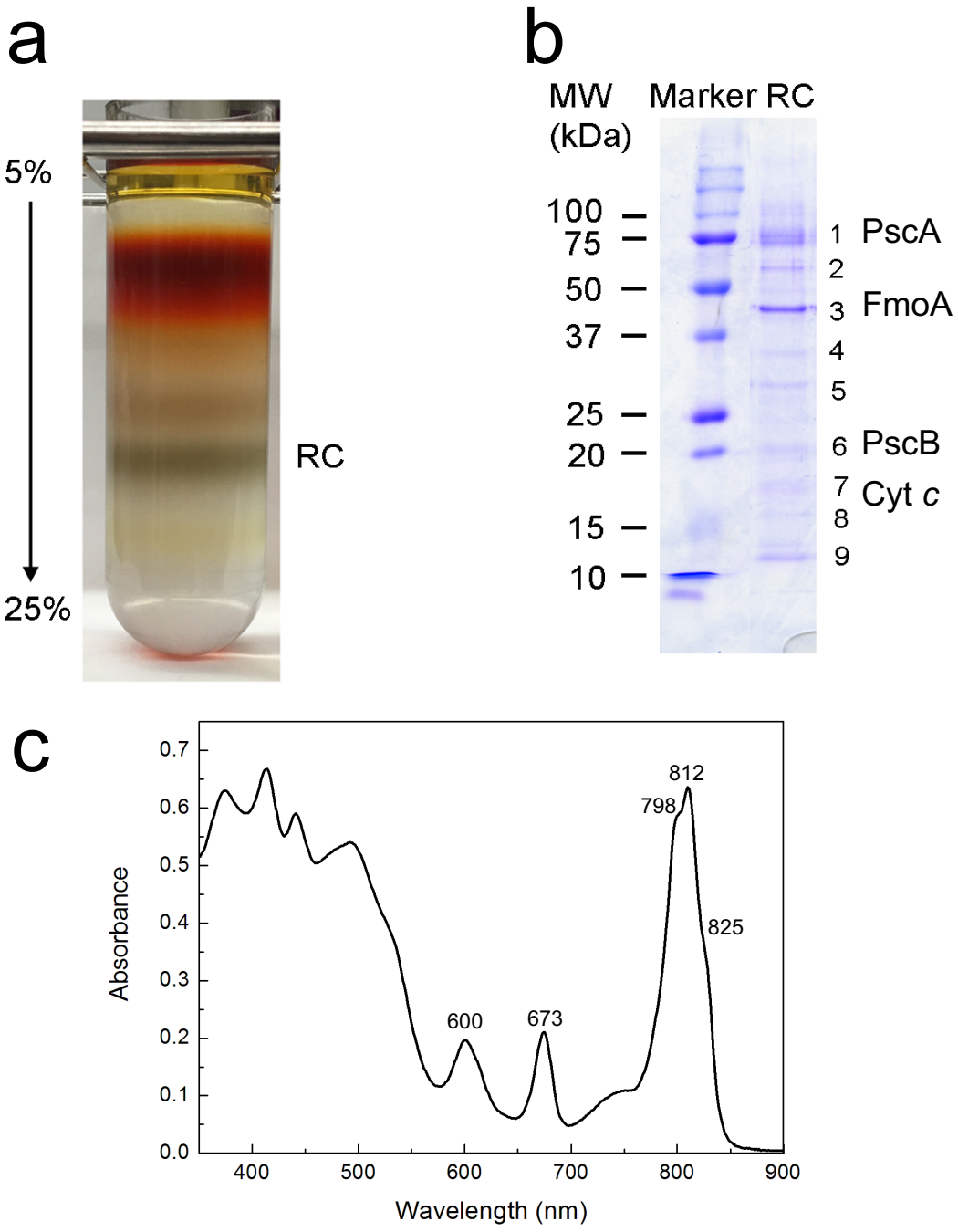
a
5%
25%
RC
b
MW
(kDa)
Marker
RC
100
75
50
37
25
20
15
10
1 PscA
2
3 FmoA
4
5
6 PscB
7 Cyt c
8
9
c
Absorbance
0.0
0.1
0.2
0.3
0.4
0.5
0.6
0.7
400
500
600
700
800
900
Wavelength (nm)
600
673
798
812
825

Figure 2

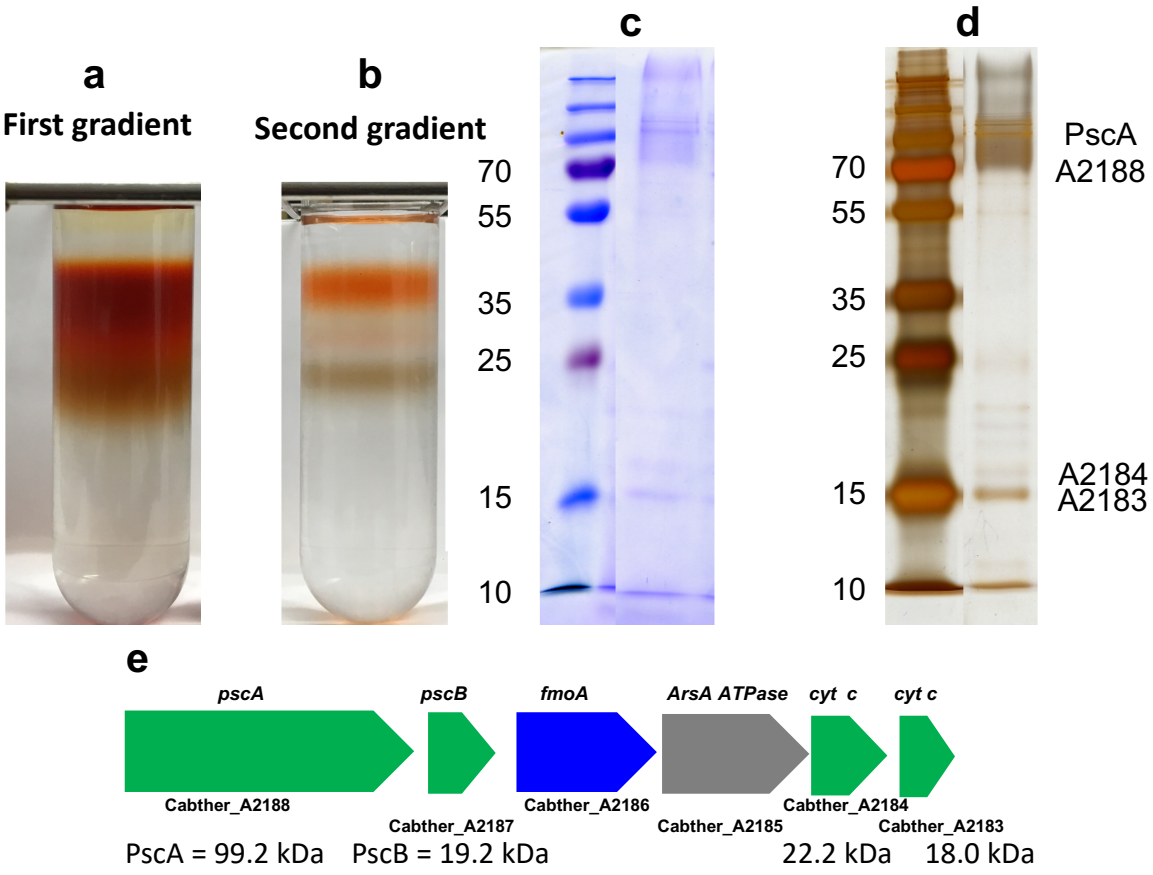
a
First gradient
b
Second gradient
c
d
70
55
35
25
15
10
PscA
A2188
A2184
A2183
e
pscA
pscB
fmoA
ArsA ATPase
cyt c
cyt c
Cabther_A2188
Cabther_A2187
Cabther_A2186
Cabther_A2185
Cabther_A2184
Cabther_A2183
PscA = 99.2 kDa
PscB = 19.2 kDa
22.2 kDa
18.0 kDa

Figure 3

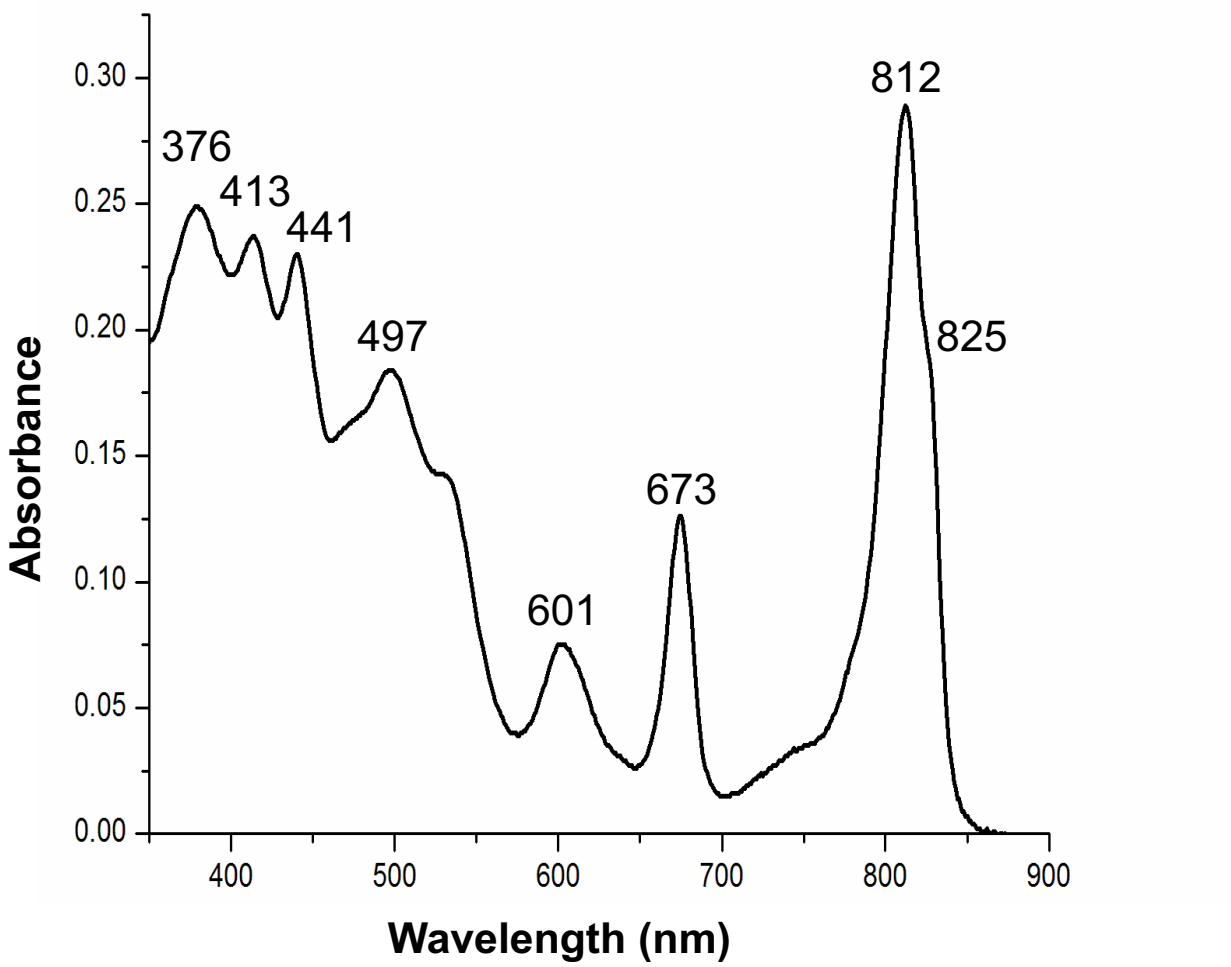
Absorbance
Wavelength (nm)
0.00
0.05
0.10
0.15
0.20
0.25
0.30
400
500
600
700
800
900
376
413
441
497
601
673
812
825

Figure 4

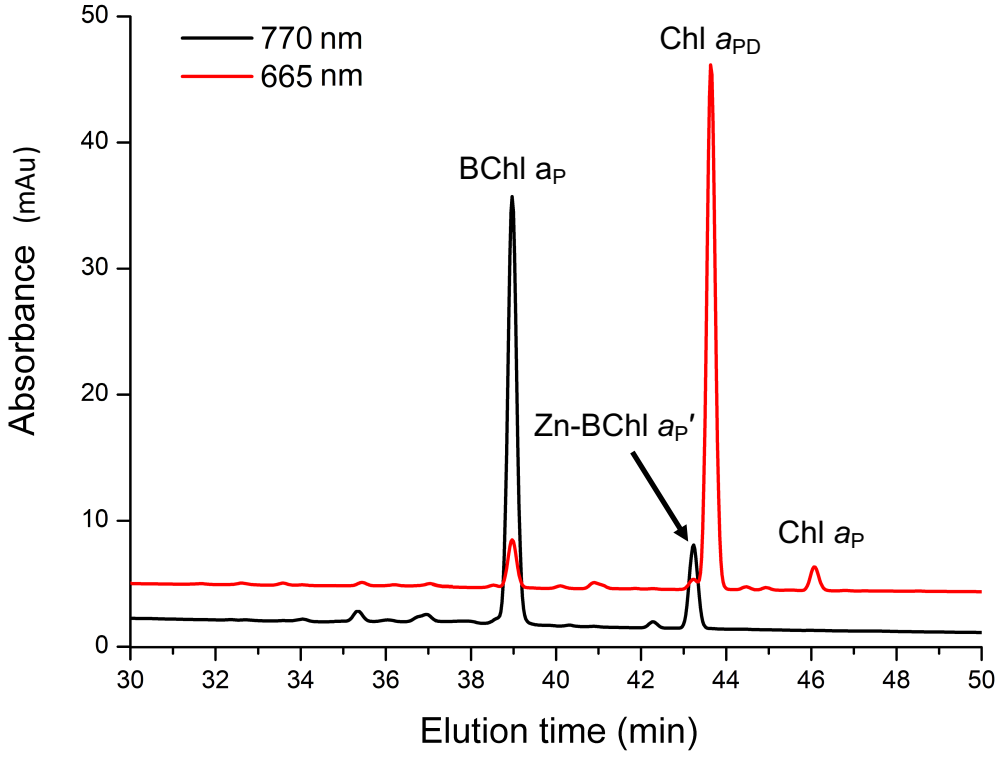
770 nm
665 nm
Chl a_{PD}
BChl a_P
Zn-BChl a_P'
Chl a_P
Absorbance (mAu)
Elution time (min)
0
10
20
30
40
50
30
32
34
36
38
40
42
44
46
48
50

Figure 5

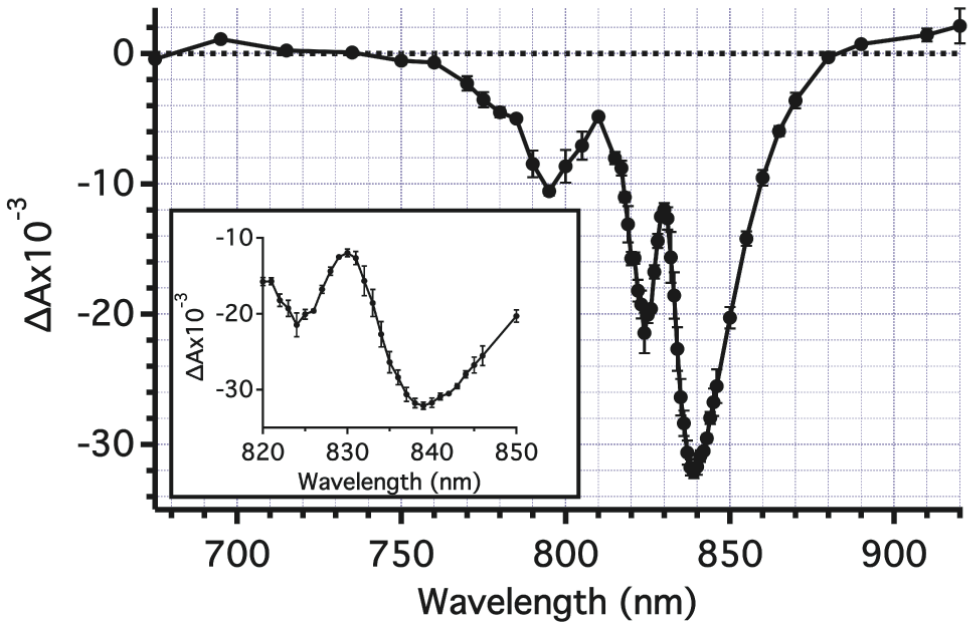
0
-10
-20
-30
ΔAx10^-3
700
750
800
850
900
Wavelength (nm)
-10
-20
-30
ΔAx10^-3
820
830
840
850
Wavelength (nm)

Figure 6

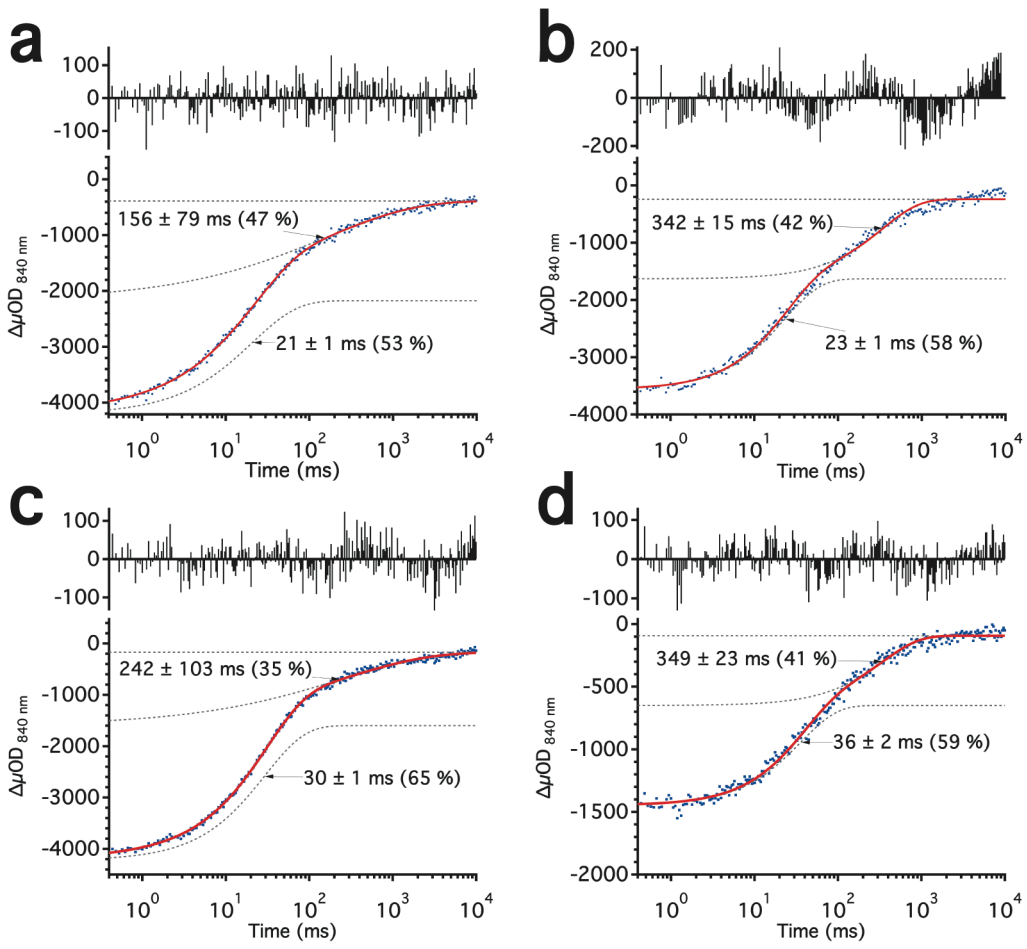
a
156 ± 79 ms (47 %)
21 ± 1 ms (53 %)
b
342 ± 15 ms (42 %)
23 ± 1 ms (58 %)
c
242 ± 103 ms (35 %)
30 ± 1 ms (65 %)
d
349 ± 23 ms (41 %)
36 ± 2 ms (59 %)
ΔμOD 840 nm
Time (ms)

Figure 7

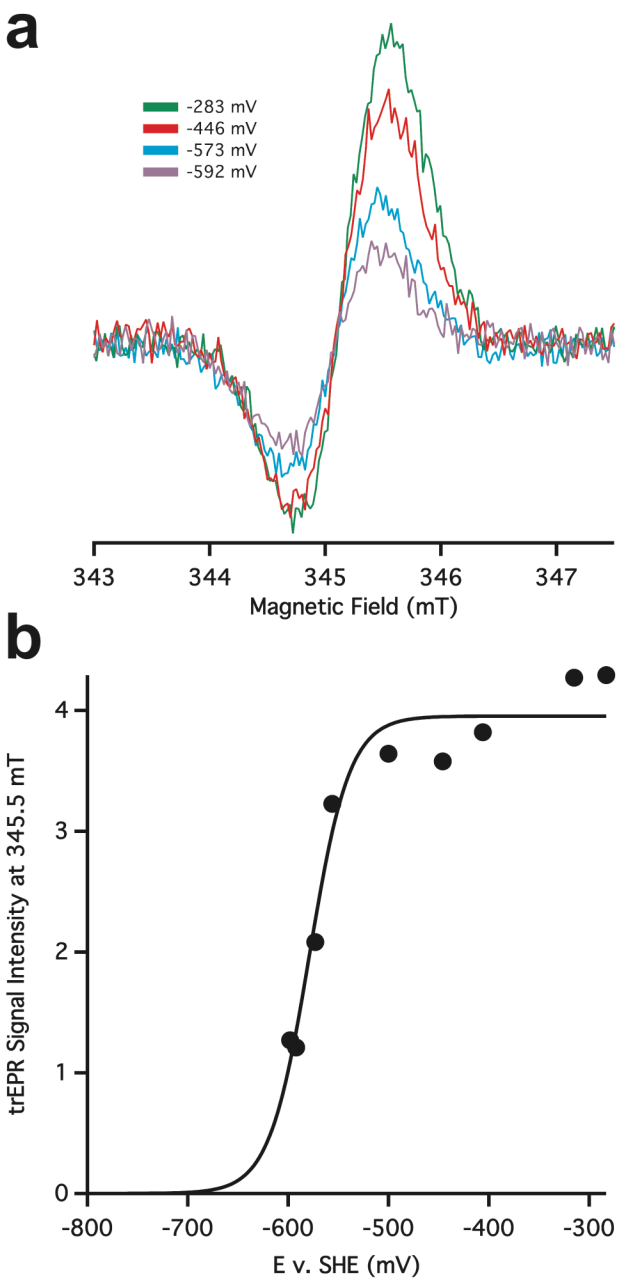
a
-283 mV
-446 mV
-573 mV
-592 mV
343
344
345
346
347
Magnetic Field (mT)
b
trEPR Signal Intensity at 345.5 mT
0
1
2
3
4
-800
-700
-600
-500
-400
-300
E v. SHE (mV)

Figure 8

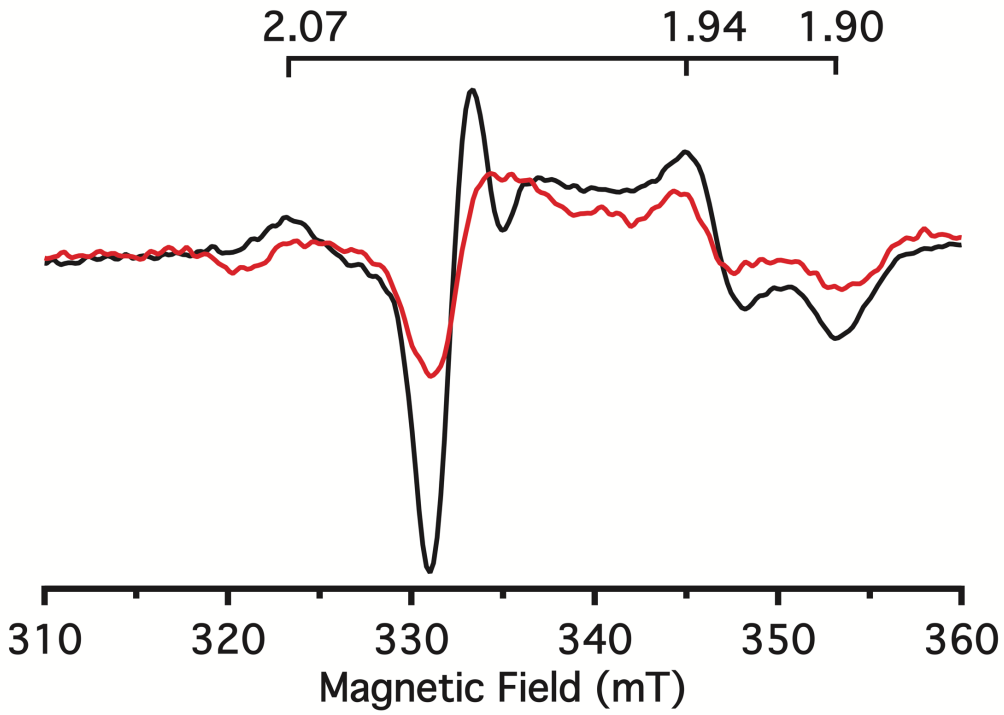

Figure 9

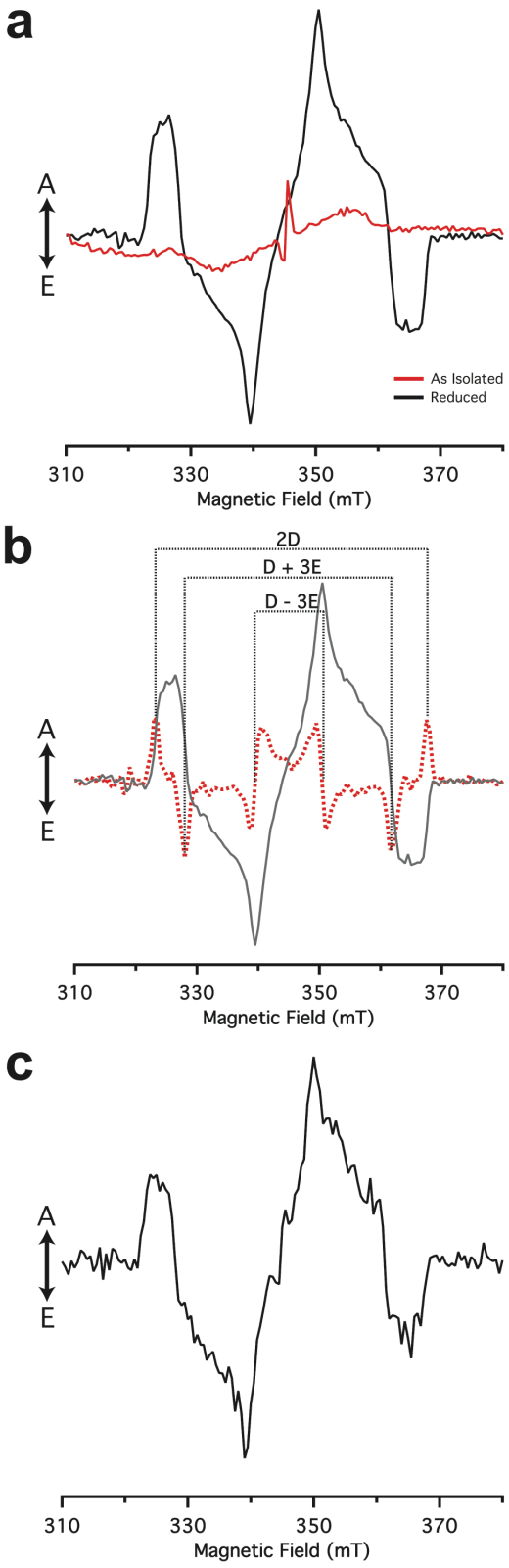
a
A
E
As Isolated
Reduced
310
330
350
370
Magnetic Field (mT)
b
2D
D + 3E
D - 3E
A
E
310
330
350
370
Magnetic Field (mT)
c
A
E
310
330
350
370
Magnetic Field (mT)

Figure 10